



HAL
open science

Trace element systematics in cold seep carbonates and associated lipid compounds

Xudong Wang, Germain Bayon, Jung-Hyun Kim, Dong-Hun Lee, Dahae Kim, Bleuenn Guéguen, Marie-Laure Rouget, Jean-Alix J-A Barrat, Laurent Toffin, Dong Feng

► **To cite this version:**

Xudong Wang, Germain Bayon, Jung-Hyun Kim, Dong-Hun Lee, Dahae Kim, et al.. Trace element systematics in cold seep carbonates and associated lipid compounds. *Chemical Geology*, 2019, 528, pp.119277 -. 10.1016/j.chemgeo.2019.119277 . hal-03487202

HAL Id: hal-03487202

<https://hal.science/hal-03487202>

Submitted on 20 Dec 2021

HAL is a multi-disciplinary open access archive for the deposit and dissemination of scientific research documents, whether they are published or not. The documents may come from teaching and research institutions in France or abroad, or from public or private research centers.

L'archive ouverte pluridisciplinaire **HAL**, est destinée au dépôt et à la diffusion de documents scientifiques de niveau recherche, publiés ou non, émanant des établissements d'enseignement et de recherche français ou étrangers, des laboratoires publics ou privés.



Distributed under a Creative Commons Attribution - NonCommercial 4.0 International License

1 **Trace element systematics in cold seep carbonates and associated lipid**
2 **compounds**

3

4 Xudong Wang^{a,b,g,h}, Germain Bayon^b, Jung-Hyun Kim^c, Dong-Hun Lee^d, Dahae Kim^c, Bleuenn
5 Guéguen^e, Marie-Laure Rouget^e, Jean-Alix Barrat^e, Laurent Toffin^f, Dong Feng^{a,g}

6

7 ^a Key Laboratory of Ocean and Marginal Sea Geology, South China Sea Institute of Oceanology,
8 Chinese Academy of Sciences, Guangzhou 510301, China

9 ^b IFREMER, Marine Geosciences Unit F-29280 Plouzané, France

10 ^c KOPRI Korea Polar Research Institute, 26 Songdomirae-ro, Yeonsu-gu, Incheon 21990, South
11 Korea

12 ^d Hanyang University, 55 Hanyangdaehak-ro, Sangrok-gu, Ansan 15588, Republic of Korea

13 ^e Laboratoire Géosciences Océan, Université de Bretagne Occidentale et Institut Universitaire
14 Européen de la Mer, Place Nicolas Copernic, 29280 Plouzané, France

15 ^f IFREMER, UMR6197, Laboratoire Microbiologie des Environnements Extrêmes, F-29280
16 Plouzané, France

17 ^g Innovation Academy of South China Sea Ecology and Environmental Engineering, Chinese
18 Academy of Sciences, Guangzhou 510301, China

19 ^h University of Chinese Academy of Sciences, Beijing 100049, China

20

21

22

23 Corresponding authors:

24 Germain Bayon (gbayon@ifremer.fr), Dong Feng (feng@scsio.ac.cn),

25

26

27 Word count: 7,298

28

29 Revised manuscript submitted to Chemical Geology

30

31 **Abstract**

32 Seeping of methane-rich fluids at submarine cold seeps drives intense microbial activity and
33 precipitation of authigenic carbonates. Some trace elements play an important role in the
34 biogeochemical processes operating at cold seeps, especially as specific enzymatic co-factors
35 related to methanogenesis and the anaerobic oxidation of methane (AOM). However, it is unclear
36 whether microbial trace metal utilization can be traced by the geochemical composition of seep
37 carbonates. In this study, we analyzed a series of authigenic carbonate samples recovered from
38 various seep settings worldwide and report for the first time trace element concentrations for total
39 lipid fractions, combined with biomarker analyses and determination of elemental abundances in
40 associated inorganic mineral phases (carbonate phases, sulfides, organic compounds and detrital
41 fractions). Our results indicate marked enrichments of Co, Ni, Cu, Mo and W in the archaeal and
42 bacterial lipids associated with authigenic carbonates, which can all be ascribed to previously
43 identified enzymatic pathways. In addition to the microbial communities involved in AOM, which
44 most likely control specific lipid-bound enrichments of Co, Ni, Mo and W in seep carbonates, Cu
45 was found to display higher concentrations in the lipid fractions extracted from a few authigenic
46 carbonate samples formed closer to the sediment-water interface, hence possibly related to the
47 presence of aerobic methane-oxidizing bacterial assemblages in the near seafloor environment.
48 While the above mentioned trace metals are relatively enriched in all studied inorganic and
49 organic fractions, the very low W concentrations measured in carbonate phases, combined with
50 their pronounced enrichment in associated lipid fractions and inferred microbial requirement,
51 suggest that tungsten depletion in pore waters could possibly act as a limiting factor on AOM at
52 cold seeps. Finally, two other trace elements (Li and Ti) also displayed particular enrichments in
53 studied lipid fractions, which, despite no reported evidence, could possibly indicate that they are
54 also involved as metalloenzymes in microbial methane oxidation processes at cold seeps.

55

56

57 **Key words:** seep carbonate; lipid compounds; trace elements; tungsten; nickel; cobalt;
58 molybdenum

59

60

61 **1. Introduction**

62 The seepage of methane-rich fluids at ocean margins sustains abundant chemosynthetic seafloor
63 ecosystems, which rely on the use of reduced chemical compounds (Levin, 2005). Fluid seepage is
64 accompanied by intense microbial activity at cold seeps, leading to precipitation of authigenic
65 minerals, such as carbonates and sulfides, and development of microbial mats close to the seafloor
66 (Sibuet and Olu, 1998; Peckmann et al., 2001; Joye et al., 2004). Microbial communities
67 prospering in cold seep environments support the highest biomass in deep-sea ecosystems, with up
68 to 10^{12} cells per cm^3 (Michaelis et al., 2002). The dominant microbial processes at cold seeps is
69 the anaerobic oxidation of methane (AOM) coupled to sulfate reduction. Until recently, it was
70 generally thought that AOM was mainly coupled with sulfate reduction in anoxic sediments, both
71 processes being driven by a consortium of archaea and bacteria assemblages, respectively (e.g.
72 Boetius et al., 2000). However, over the past few years, several studies have demonstrated that
73 microorganisms could also use nitrate or metal oxides to promote methane oxidation at cold seeps
74 (Raghoebarsing et al., 2006; Beal et al., 2009; Scheller et al., 2010; Glass et al., 2014). Manganese

75 (Mn) and iron (Fe)-rich oxyhydroxides have been identified as electron acceptors for AOM (Beal
76 et al., 2009), but other trace metals, such as nickel (Ni), cobalt, (Co), molybdenum (Mo) and
77 tungsten (W) are also involved in methane oxidation processes as enzymatic co-factors (Krüger et
78 al., 2003; Glass et al., 2014). Trace metals are also suspected to have played key roles in the
79 long-term evolution of microbial activity through geologic time (Anbar, 2008; Konhauser et al.,
80 2009; Reinhard et al., 2013). For example, an important drop in dissolved Ni concentrations in
81 Precambrian oceans after about 2.5 Ga, as a consequence of the progressive decrease in the
82 production of Ni-rich volcanic rocks (komatiites) on Earth, would have led to reduced activity of
83 methanogenic microbes, with possibly global impact on the composition of the atmosphere
84 (Konhauser et al., 2009). To date, however, and despite their potential importance in AOM, very
85 little is known about the utility of trace elements for microbial activity and metabolism at cold
86 seeps.

87
88 Trace metals are essential in biological systems, playing key roles in microbially-driven
89 biogeochemical processes. In addition to iron, other transition metals (Zn, Mn, Co, Ni, Cu, V, Mo
90 and W) have been identified in proteins and enzymes involved in the metabolism of
91 sulfate-reducing bacteria or methanogenic and methanotrophic archaea (e.g. Scherer et al., 1983;
92 Krüger et al., 2003; Barton et al., 2007; Scheller et al., 2010; Glass and Orphan, 2012; Glass et al.,
93 2014; 2018). Amongst trace metals, Ni appears to play a particularly important role in anaerobic
94 methanotrophy and methanogenesis (Krüger et al., 2003; Scheller et al., 2010; Thauer et al., 2010).
95 The microbial communities involved in AOM also utilize other essential trace metals, such as Co,
96 W and Mo (e.g. Glass et al., 2014; 2018). Many of these findings have been obtained from culture
97 experiments, but little is known about how microbial activity at cold seeps may be affected by
98 changes in trace metal bioavailability from one site to another. Transition metals can be intensively
99 scavenged during precipitation of authigenic minerals, such as sulfides and carbonates in methane
100 seepage areas (Bayon et al., 2011a; Lemaitre et al., 2014), which can severely reduce their
101 availability to microbial communities (Glass and Orphan, 2012). Recent investigations have also
102 suggested that light rare earth elements (REE) could be essential for methanotrophs as co-factors
103 in the methanol dehydrogenase enzyme (Pol et al., 2014; Jahn et al., 2018; Picone and den Camp,
104 2019). This previously unsuspected biological role of REE for methanotrophic and methylotrophic
105 bacteria was also demonstrated in a recent study that investigated the methane plumes emitted in
106 the Gulf of Mexico following the Deepwater Horizon blowout, which revealed significant
107 depletion of light REE (La, Ce, Pr, and Nd) relative to the surrounding seawater (Scheller et al.,
108 2017).

109
110 At submarine methane seeps, authigenic carbonates are a by-product of microbially-mediated
111 AOM (Aloisi et al., 2000; 2002), which can hence provide unique information on past seepage
112 activity and associated environmental parameters (Feng et al., 2015). Extensive work has been
113 conducted on the geochemistry of authigenic carbonates and associated sediments, in both modern
114 and ancient seep settings. Previous studies have focused on both conventional and
115 non-conventional stable isotopes and radiogenic isotopes (including U-Th dating methods) to
116 provide constraints on both fluid sources and the timing of fluid seepage events at ocean margins
117 (Peckmann et al., 2001; Pierre and Fouquet, 2007; Ge and Jiang, 2013; Bayon et al., 2015; Hu et
118 al., 2015a; Sun et al., 2015; Lu et al., 2017).

119

120 Trace elements in seep carbonates have been mostly used as proxies for the source of fluids, but
121 also to provide information on redox conditions. Both carbonates and associated sediments at
122 methane seeps display relatively high elemental concentrations, suggesting that they act as a sink
123 for many trace elements, such as Mo and rare earth elements (Sato et al., 2012; Lemaitre et al.,
124 2014; Hu et al., 2015b). It is generally assumed that trace element distribution patterns in
125 authigenic carbonates reflect the composition of ambient pore waters. However, fractionation of
126 REE can occur upon carbonate precipitation, in response to changing carbonate alkalinity levels in
127 pore waters, which affect REE complexation by organic and carbonate ligands (Himmler et al.,
128 2010; Rongemaille et al., 2011). The degree of Ce enrichment or depletion in modern and ancient
129 seep carbonates, relative to its trivalent REE neighbors (the so-called Ce-anomaly), has been also
130 used as a paleo-redox tracer (Feng et al., 2009).

131

132 Comparatively, there have been very few studies dedicated to trace elements in organic
133 compounds at cold seeps. Freslon et al. (2014) reported REE concentrations for organic
134 compounds chemically leached from a series of marine sediment samples, including sediments
135 recovered from active seep sites worldwide, showing strong REE enrichments in cold seep
136 sediments. This study suggested that a significant fraction of sedimentary organic matter at these
137 sites was derived from chemosynthetic processes recycling REE-enriched pore waters. Over the
138 past decades, lipid biomarker analysis of seep carbonates has provided a wealth of information on
139 the nature of microbial communities involved in carbonate precipitation (e.g. Aloisi et al., 2002;
140 Himmler et al., 2015; Guan et al., 2016). However, to the best of our knowledge, the trace element
141 geochemistry of lipids preserved in authigenic carbonates has never been investigated so far.

142

143 In this study, we aimed at characterizing the trace element geochemistry of lipids preserved in
144 authigenic carbonates, in order to provide independent information on the utility of trace metals to
145 microbial activity at methane seeps. In contrast to the trace element signatures preserved by
146 inorganic phases in cold seep carbonates, which mostly reflect the composition of ambient pore
147 waters and local redox conditions (Hu et al., 2015b), our working hypothesis is that any particular
148 elemental enrichments/anomalies in the lipid fractions reflect trace metal requirements for
149 microbial metabolism. To this purpose, we have analysed a series of authigenic carbonate samples
150 from various active seeps worldwide, reporting trace element data for both carbonate and lipid
151 fractions. Our approach combines biomarker and inorganic element analyses of total lipid
152 fractions extracted from a series of carbonate crusts, together with determination of trace element
153 contents in associated mineral phases (carbonates, sulfides and organic compounds, detrital
154 fractions), separated by sequential chemical leaching. The aim of this study was to detect specific
155 enrichments that would be indicative of preferential metal utilization by microorganisms.

156

157

158 **2. Materials and methods**

159 *2.1. Sample preparation*

160 A total of 19 seep carbonate samples from five different active seepage areas worldwide (Congo
161 fan, Nile deep-sea fan, Niger fan, Eastern Mediterranean Sea, Gulf of Mexico) were analyzed (Fig.
162 1). Most of these samples have been previously characterized for carbonate mineralogy and/or

163 stable isotopes (Table 1; see references therein). For clarity, note that we re-labelled the name of
164 the samples in this study (Fig. 1; Table 1).

165

166 2.2. Pretreatment procedures

167 Carbonate chips were first cleaned with ultrapure Milli-Q (MQ) water and dried, prior to being
168 crushed into powder using an agate and mortar. Samples were split into two aliquots of about 5 g
169 each for lipid biomarker extraction and analyses at the Korea Polar Research Institute (KOPRI)
170 and sequential chemical leaching at IFREMER, respectively.

171

172 Upon formation at cold seeps, authigenic carbonates can incorporate substantial amounts of
173 sulfide and detrital minerals from the surrounding sediment, in addition to the various organic
174 compounds related to AOM. Previous studies have shown that even a small proportion of detrital
175 contamination can significantly modify trace element abundances in carbonates (Nance and Taylor,
176 1976; Nothdurft et al., 2004, Frimmel, 2009). Therefore, selective chemical leaching methods are
177 required for investigating the geochemistry of relatively pure carbonate and organic phases,
178 without contamination from detrital and sulfide minerals (Bayon et al., 2002; Rongemaille et al.,
179 2011; Freslon et al., 2014). In this study, we used a sequential leaching procedure adapted from
180 Chao and Sanzalone (1977), Freslon et al. (2014) and Tachikawa et al. (2014), resulting in the
181 following sequence of leaching steps: 1) stepwise addition of 1M acetic acid (AA), to extract a
182 pure fraction of the most labile carbonate phases, such as aragonite and calcite; 2) 0.25M HCl, to
183 remove most carbonate minerals; 3) 5% hydrogen peroxide (H₂O₂), to extract organic compounds
184 (and possibly some sulfide minerals); 4) 3M HNO₃ to leach out pyrite minerals (and presumably
185 any residual carbonate and organic phases); 5) digestion of detrital silicate minerals using
186 concentrated HF + HCl.

187

188 For the first leaching step, about 50 mg of powdered carbonate samples were placed into an
189 acid-cleaned 15 ml polyethylene centrifuge tube, together with 500 µl ultrapure MQ water. After
190 addition of a Tm spike (see details below), carbonates were slowly dissolved with stepwise (100
191 µl) addition of ultraclean 1M AA solution. The next 100 µl aliquot was added once the bubbling
192 has ceased; this step being repeated until addition of a total of 1 ml 1M AA, hence corresponding
193 to a resulting leaching solution of about 3.8 wt%. This gentle leaching step was initially developed
194 for measuring neodymium (Nd) isotopic ratios in foraminifera (Tachikawa et al., 2014). It ensures
195 partial dissolution of the most soluble carbonate phases (aragonite, calcite) with limited
196 contamination from silicate and sulfide minerals. The tube was then centrifuged at 3800 rpm for 4
197 minutes, and the supernatant was transferred into a cleaned polytetrafluoroethylene (PTFE) vial,
198 prior to evaporation and preparation for ICP-MS analyses.

199

200 Next, a four-stage sequential leaching procedure was conducted on our series of carbonate
201 samples, starting from about 500 mg of bulk powdered samples. Following a protocol adapted
202 from Freslon et al. (2014), the most soluble carbonate phases were first dissolved using 0.25M
203 HCl in a PTFE vial left at room temperature for 3 hours. After centrifugation of the supernatant,
204 this leaching step was repeated once, and the remaining residue was rinsed twice with ultrapure
205 MQ water, and dried overnight in the oven.

206

207 The remaining dried residues were weighed, crushed, and placed into corresponding PTFE vials.
208 The next leaching step corresponded to the addition of a mixed solution of 5% H₂O₂ + 0.01M
209 HNO₃, together with Tm spike, in order to oxidize organic matter (and possibly the easily
210 dissolvable sulfide phases; Dold, 2003). The vials were placed on a mechanical shaker and left at
211 room temperature for 48 hours. The solutions were centrifuged at 3500 rpm for 3 min and the
212 supernatants were transferred into acid-cleaned 15 ml centrifuge tubes after filtration using
213 high-density polyethylene (HDPE) 0.2 μm filters. After evaporation onto the hot plate, the
214 organic-rich samples were digested overnight with concentrated nitric (140°C), prior to being
215 evaporated again and prepared for ICP-MS analyses.

216

217 Next, the residues left after the H₂O₂ leaching step were rinsed with ultrapure MQ water, dried
218 overnight, crushed and weighed. The next leaching step was performed using 3M HNO₃, aiming at
219 dissolving a substantial fraction of sulfide minerals (Chao and Sanzalone, 1977), but also,
220 presumably, any residual carbonate and organic phases that would have been left after the 0.25M
221 HCl and 5% H₂O₂ steps, together with probably some silicate minerals. Chao and Sanzalone (1977)
222 investigated various chemical treatments for dissolving primary sulfide minerals in sediments,
223 showing that the use of moderately diluted HNO₃ solutions was quite effective for dissolving
224 pyrite, hence our decision to use 3M HNO₃ for this leaching step. After addition of a Tm spike,
225 3M HNO₃ was added to the samples and left on a mechanical shaker overnight. The leachates
226 were separated by centrifugation (3800 rpm for 4 min) and transferred into an acid cleaned Teflon
227 vial prior to preparation for ICP-MS analyses. The residues were rinsed with ultrapure MQ water,
228 dried and crushed. Finally, about 15 mg of the final residual fractions were digested on the
229 hotplate (140°C for 5 days) with concentrated HF and HCl.

230

231 2.3. ICP-MS analysis

232 All trace element analyses were performed at the Pôle Spectrométrie Océan (Brest, France) on an
233 Element XR ICP-MS. Polyatomic oxide and hydroxide interferences on the REE were corrected
234 using oxide formation rates determined by analyzing solutions of MQ-H₂O, Ba + Ce, Pr + Nd and
235 Sm + Tb at the beginning of each measurement session and applied to all samples. Elemental
236 concentrations were calculated using the Tm addition method (Barrat et al., 1996; Bayon et al.,
237 2009). Over recent years, this method has been successfully applied to and validated for a wide
238 range of geological samples, including detrital and organic sediments (Freslon et al., 2014; Bayon
239 et al., 2015), carbonates (Rongemaille et al., 2011), seawater (Bayon et al., 2011b; Freslon et al.,
240 2011). Briefly, raw trace element data were calibrated against an unspiked (no added Tm)
241 BHVO-2 reference solution run after every three samples to correct for instrumental drift. The
242 BHVO-2 values used for the calculations (Barrat et al., 2012; Jochum et al., 2016) are given in
243 Table 1. Trace element abundances in the samples are then calculated using the mass of sample
244 spiked with Tm and the amount of Tm added. The internal precision on all measurements was
245 generally better than 5%. Repeated analyses of the JLs-1 (Triassic limestone) reference material
246 were also performed, with a precision of < 10% for most trace elements (Table 2), except for Li
247 (11.8% RSD), Ti (61% RSD) and Zr (17% RSD). Due to high Ba/REE ratios, several carbonate
248 samples (including JLs-1) analyzed displayed anomalously high Eu (and to a lesser extent Gd)
249 concentrations as a result of under-corrected interferences, hence these two elements were not
250 reported.

251

252 2.4. Lipid biomarker analysis

253 Detailed procedures for lipid biomarker analyses were previously described by Lee et al. (2018).
254 Briefly, total lipid fractions were extracted 3 times with dichloromethane (DCM):methanol
255 (MeOH) (2:1). One-half of the total lipid extract (TLE) was dried over anhydrous Na₂SO₄ and
256 treated with tetrabutylammonium sulfite reagent to remove elemental sulfur. The TLE was
257 chromatographically separated into apolar and polar fractions over an Al₂O₃ (activated for 2 h at
258 150°C) column. The apolar fraction was eluted using hexane:DCM (9:1), and 40 µL of
259 5α-androstane (10 µg mL⁻¹) was added as an internal standard. The polar fraction was recovered
260 with DCM:MeOH (1:1) as an eluent and divided into two aliquots, to which either C₂₂ 7,16-diol
261 (10 µg mL⁻¹) or C₁₉ nonadecanoic acid (10 µg mL⁻¹) were added as an internal standard. Each
262 aliquot was derivatized through the procedures of silylation and methylation, prior to
263 quantification with gas chromatography (GC) and identification with gas chromatography-mass
264 spectrometry (GC-MS). GC and GC-MS conditions were as described by Lee et al. (2018).
265 Molecular compounds were determined by comparing their mass spectral fragmentation patterns
266 and retention times with previously published data (e.g. Stadnitskaia et al., 2008; Lee et al., 2018).

267

268 2.5. Principal component analysis (PCA)

269 Based on the fractional abundances of microbial lipids, principal component analysis (PCA) was
270 performed using R software version 3.4.2 (package information; FactoMineR) to provide a general
271 view of the variability of the microbial lipid distributions. For the statistical analysis, gaps in the
272 data set were filled as described by Yunker et al. (2005). Briefly, in cases when some of microbial
273 lipids were not determined, a value of one-half of minimum value detected for that variable in the
274 whole data was set as the limit of detection. These values then were replaced by a random number
275 between zero and the limit of detection. Finally, samples were transformed using Z-score
276 normalization to remove artefacts related to the large differences in concentration between
277 samples.

278

279

280 3. Results

281 Trace element data for carbonate (1M AA leachates), sulfide-rich (3M HNO₃ leachates), detrital
282 (HF-HCl digestion), bulk organic (5% H₂O₂ leachates) and lipid fractions are reported in Table 3
283 and described below in separate sections. For clarity, results are also presented as normalized
284 values (Fig. 2 and 3), which helps identifying any particular trace element enrichment or depletion
285 in studied mineral and organic fractions. In addition, archaeal and bacterial lipid biomarker data
286 were presented in Table 4 and described in a separate section.

287

288 3.1. Carbonate phases (aragonite, calcite): 1M AA leachates

289 Studied carbonate samples display a large range of Sr concentrations (between ~300 to 15500
290 mg/kg). As already described previously (e.g. Jørgensen, 1992; Savard et al., 1996; Bayon et al.,
291 2007), aragonite-rich samples are characterized by much higher Sr contents (between ~ 8000 to
292 15500 mg/kg), than calcite- or dolomite-dominated samples (generally < 3000 mg/kg). Other
293 elements also display large concentration ranges, for example for Co (between 0.03 - 2.42 mg/kg),
294 Mo (0.05 - 5.13 mg/kg) and Nd (0.10-10.3 mg/kg). Compared to the marine limestone standard

295 (JLs-1), cold seep carbonate samples are generally characterized by much higher trace element
296 contents (Fig. 2a), many of them (Li, Sc, transition metals, Sr, Mo, REE, Pb and Th) being up to a
297 few hundred times more enriched. In contrast, three elements (Ti, Ba and W) display much lower
298 concentrations (up to 100 times depleted compared to JLs-1).

299

300 *3.2. Sulfide minerals: 3M HNO₃ leachates*

301 The concentrations for Ca in 3M HNO₃ leachates range between 37088 and 115006 mg/kg, hence
302 being significantly lower than in 1M AA leachates. Selected trace element concentrations also
303 display a very large range of values (between 2.0 - 36.4 mg/kg for Ti; 0.03 - 3.84 mg/kg for Co;
304 0.05 - 2.16 mg/kg for Mo; and 0.06 - 8.37 mg/kg for Nd). Trace element data for 3M HNO₃
305 leachates are normalized to the 1M AA leachate data in order to evaluate their degree of
306 enrichment or depletion relative to corresponding carbonate phases. Apart from Ca and Sr, and to
307 a lesser extent Mn, Ba, REE, W and U, which are generally depleted in 3M HNO₃ leachates
308 compared to 1M AA leachates, most trace elements are enriched up to 10 times (Co, Ni, Zn, Rb,
309 Zr, Mo, Hf, and Th) or 100 times (Ti, Cu, Pb) in the sulfide-rich leached fractions of studied
310 carbonate samples.

311

312 *3.3. Detrital silicate fractions: conc. HF+HCl acid digestion*

313 Measured Ca concentrations for the residual silicate fractions associated with seep carbonates
314 (between 679 - 6165 mg/kg) are much lower than in any other studied mineral/organic phases.
315 This shows that our sequential chemical procedure was effective at quantitatively removing most
316 carbonate material. Many trace elements generally display a relatively small range of
317 concentrations (Table 3). Trace element abundances in residual silicate fractions can be
318 normalized to reference shale values, such as the Post Archean Australian shale composite (PAAS;
319 Taylor and MacLennan, 1985), in order to identify particular enrichment or depletion relative to an
320 average bulk sediment composition. Several elements, such as Ca, Mn, Cu, Sr, Ba and Pb, are
321 significantly depleted in the residual silicate fraction of seep carbonates relative to PAAS, but this
322 simply reflects, at least to some extent, the fact that PAAS is a bulk reference composite sediment
323 that also contains non-silicate phases (carbonates) enriched in these particular elements. However,
324 a few samples display much higher PAAS-normalized concentrations for Ba and Sr (up to 30
325 times), which reflect the presence of barite, i.e. a common authigenic mineral at cold seeps that is
326 resistant to most chemical leaching procedures, including digestion using concentrated HF-HCl
327 solutions. In addition, many residual silicate fractions are also characterized by pronounced
328 PAAS-normalized enrichments in Mo, also up to 30 times.

329

330 *3.4. Bulk organic compounds: 5% H₂O₂ leachates*

331 The 5% H₂O₂ leachates are generally characterized by very high Ca concentrations (up to ~570000
332 mg/kg), indicating that carbonates represent the dominant phase extracted during this leaching step.
333 This is also reflected by the high Sr (up to 6300 mg/kg) and Mg (up to 127000 mg/kg)
334 concentrations determined in the same solutions. As a consequence, it appears difficult to draw
335 any conclusions regarding the partitioning of selected trace elements into the organic compounds
336 hosted by seep carbonates. However, normalizing the 5% H₂O₂ leachate data to those obtained for
337 1M AA (carbonates) and 3M HNO₃ (sulfides) leachates can still help identifying some particular
338 elements that would be more specifically associated with the organic component hosted by seep

339 carbonates. This is the case for at least three elements (V, Mo and W), which all show pronounced
340 normalized-enrichments (up to a thousand times) in 5% H₂O₂ leachates (Fig. 3a and 3b). To a
341 lesser extent, the transition metals (Co, Ni, Cu, Zn) also appear to be enriched (up to 10-100 times)
342 in 5% H₂O₂ leachates compared to 1M AA and 3M HNO₃ leachates.

343

344 3.5. Total lipids

345 In contrast to the 5% H₂O₂ leachates, the extracted lipid fractions display much lower Ca
346 concentrations (between 2270 - 51045 mg/kg, with an average of 15000 mg/kg), hence indicating
347 limited carbonate dissolution (generally < 5 wt%). Amongst the other studied elements, Li
348 concentrations range from 6.6 to 32.6 mg/kg; Ti from 1.1 to 29.6 mg/kg; Cu from 0.9 to 37.9
349 mg/kg; Mo from 0.1 to 3.0 mg/kg and W from 0.01 to 0.08 mg/kg. In comparison, REE display
350 very low concentrations with Nd concentrations between ~0.1 and 1.0 mg/kg. Compared to the
351 abundances determined in carbonate (1M AA) and sulfide (3M HNO₃) leachates, elemental
352 concentrations in lipid fractions are very low for the following elements: Ca, Sc, Mn, REE, Th and
353 U (Fig. 3c and 3d). In contrast, some trace elements, such as Li, Ti, V, Cu, Zn, Mo, and W exhibit
354 clearly identifiable enrichments (up to 100 times) in lipids.

355

356 3.6. Microbial lipid biomarkers

357 Concentrations of archaeal and bacterial lipids showed large variations in studied authigenic
358 carbonates (Table 4). For archaeal lipids, the irregular tail-to-tail isoprenoids such as crocetane,
359 which was co-eluted with phytane, pentamethylcosane (PMI), and polyunsaturated
360 pentamethylcosenes (PMEs) were detected, varying between 0.03 and 0.25 µg/g dry weight (dw),
361 0.02 to 0.25 µg/g dw, and 0.01 to 0.49 µg/g dw, respectively. Moreover, isoprenoid dialkyl
362 glycerol diethers (isoprenoid DGDs), such as archaeol and *sn*-2-hydroxyarchaeol, were the most
363 predominant archaeal lipids in studied samples, displaying concentration ranges between 0.01–
364 6.97 µg/g dw, and 0.03–22.13 µg/g dw, respectively. For bacterial lipids, non-isoprenoid DGDs
365 with anteiso pentadecyl moieties or cyclopropyl groups attached at both the *sn*-1 and *sn*-2
366 positions were identified, ranging from 0.01 to 1.07 µg/g dw. Among FAs detected, saturated FAs
367 (e.g. C16:0 and C18:0) were most predominant, with the range of 0.06–1.99 µg/g dw (Table 4).
368 Other FAs (e.g. *i*-C15:0, *ai*-C15:0, C16:1 ω 7, C18:1 ω 9 and C18:1 ω 7) were approximately 3 to 10
369 times lower in concentrations (0.01 to 0.16 µg/g dw) compared to saturated FAs.

370

371

372 4. Discussion

373 4.1. Distribution of trace elements in authigenic carbonate phases

374 As discussed in previous studies, the distribution of trace elements in cold seep carbonates can be
375 controlled by various parameters, including mineralogy, composition of the fluids from which they
376 have precipitated from, and redox conditions (Peckmann et al, 2001; Conti et al, 2004; Bayon et al,
377 2007; Feng et al., 2009; Ge et al, 2010). In addition to Sr, which is significantly enriched in
378 aragonite compared to other carbonate phases (see section 3.1), U and Mn are also preferentially
379 incorporated into aragonite- (characterized by high Sr/Ca contents) and calcite- (low Sr/Ca)
380 dominated samples (Fig. 4a and 4b), respectively. To a large extent, the chemical composition of
381 surrounding pore waters also plays a major role in controlling trace element distribution patterns
382 in authigenic carbonates. This explains why many trace elements are enriched in cold seep

383 carbonates compared to marine bioskeletal carbonates (e.g. JLs-1 limestone; Fig. 2a). This is
384 illustrated taking the example of the REE, which also exhibit a relationship with mineralogy in a
385 Nd/Ca versus Sr/Ca plot (Fig. 4c). The abundance of REE in pore waters is generally much higher
386 than in overlying bottom waters, because of various early diagenetic processes, such as the
387 reduction of Fe-Mn oxyhydroxide phases or organic matter remineralization, which can release
388 substantial amounts of dissolved REE within the sub-surface sediment (Haley et al., 2004). Since
389 high-Mg authigenic carbonate minerals, such as dolomite, often form in relatively deeply buried
390 sulfate-depleted sediment layers (typically a few meters below the seafloor) characterized by high
391 dissolved REE contents (Soyol-Erdene and Huh, 2013), they are likely to incorporate higher
392 amounts of REE compared to mineral phases such as aragonite, which precipitate in the near
393 seafloor environment from less REE-enriched pore waters.

394

395 In addition to this source effect, the ubiquitous presence of anoxic conditions at cold seeps also
396 explains why many redox sensitive elements are typically more enriched in methane-derived
397 carbonates compared to other marine carbonate material such as JLs-1 (Fig. 2a). For instance, this
398 is the case for redox sensitive elements like Mo, U, Ni, V, Cd, Co, and Zn, which are typically
399 immobilized under anoxic conditions. In fact, many of these elements have been used in previous
400 studies for providing constraints into the redox conditions of formation of carbonate minerals
401 (Morford and Emerson, 1999; Sarkar et al., 2003). Enrichments in Mo have been reported widely
402 in many seep carbonate samples (Central Mediterranean, Cangemi et al., 2010; Vocontian Trough,
403 SE-France, Tribovillard et al., 2013; Gulf of Mexico, Hu et al., 2014; Northwestern South China
404 Sea, Liang et al., 2017; Southwestern Taiwan, Wang et al., 2019). Ge et al. (2010) also found
405 particularly high abundances of Mo, V, Co, Ni and U in authigenic carbonate samples recovered
406 from the Shenhu and Dongsha seep areas of the South China Sea compared to marine bioskeletal
407 carbonates.

408

409 In marked contrast, as shown in the results section, Ba, Ti and W often display much lower
410 abundances in studied seep carbonates relative to JLs-1 (Fig. 2a). For Ba, this depletion is best
411 explained by the fact that precipitation of authigenic barite at cold seeps acts as an effective sink
412 for pore water Ba. While previous partitioning experiments have demonstrated that Ba is
413 preferentially incorporated into aragonite compared to calcite (Pingitore Jr and Eastman, 1984),
414 our results indicate instead that Ba generally exhibit higher concentrations in calcite rather than in
415 aragonite-dominated samples (Fig. 4d). This preferential enrichment of Ba in calcite relative to
416 aragonite is most likely controlled by the availability of Ba at the depth of mineral formation (e.g.,
417 Torres et al, 2002, 2010; Snyder et al, 2007). At methane seeps, pore water Ba concentrations
418 markedly increase in the sediment column located below the depth of sulfate depletion, as a
419 consequence of barite ($BaSO_4$) dissolution. The upward diffusing resulting flux of dissolved Ba is
420 almost quantitatively precipitated into authigenic barite at the sulfate-methane transition zone
421 (SMTZ), but a minor fraction of dissolved Ba is also likely to be incorporated into the high-Mg
422 carbonate phases that form at the SMTZ when it is located well below the sediment-seafloor
423 interface. In contrast, aragonite generally forms in the sulfate-rich near seafloor environment at
424 cold seeps (Burton, 1993, Luff and Wallmann, 2003, Peckmann et al., 2009), where pore water Ba
425 contents are presumably much lower than in the deeper methanogenic sediments, hence possibly
426 explaining the relatively low Ba concentrations encountered in most aragonite-rich samples (Liang

427 et al., 2017).

428

429 The cause of Ti and W depletion in studied carbonate samples remains unclear, as these features
430 have never been described previously in the literature, at least to the best of our knowledge. This
431 will be the focus of a part of the discussion below, when interpreting the results obtained for the
432 organic fractions. One hypothesis would be that these elements have been partly re-adsorbed onto
433 residual phases during the 1M AA leaching step, thereby explaining the depleted Ti and W
434 concentrations in corresponding leachates. However, if this had been the case, one would have
435 also expected similar depletions for other particle reactive elements such as Zr and Hf. Because
436 this is not the case (Fig. 2a), we argue that the observed Ti and W depletions in carbonates simply
437 reflect their very low concentrations in surrounding pore waters at the time of carbonate
438 precipitation, as a consequence of (micro)biogeochemical processes that will be discussed below.

439

440 *4.2. Trace element enrichments associated with the presence of sulfide minerals*

441 The data obtained on 3M HNO₃ leachates allow us to identify the trace elements that are likely to
442 be preferentially associated with sulfide minerals within seep carbonates. Of course, we are well
443 aware that this leaching step is not selective and may have also led to substantial dissolution of
444 residual carbonate phases, organic compounds and silicate minerals. As a matter of fact, although
445 Ca and Sr in 3M HNO₃ leachates are significantly depleted compared to corresponding carbonate
446 phases (i.e. 1M AA leachates), their presence in 3M HNO₃ leachates clearly indicates that a
447 substantial fraction of the material dissolved by 3M HNO₃ corresponds to carbonates that were left
448 behind the previous 0.25M HCl leaching step. Similarly, a few other trace elements, such as Mn,
449 Ba, REE, W and U, almost systematically display lower concentrations in 3M HNO₃ leachates
450 relative to 1M AA solutions, showing that they are mostly depleted in sulfide minerals. In addition,
451 the pronounced enrichments displayed by elements typically associated with detrital silicates (Ti,
452 Rb, Zr and Th) clearly indicate that partial dissolution of silicate minerals occurred during the
453 leaching step. In contrast, however, the high elemental abundances determined for transition
454 metals (Co, Ni, Cu, Zn, Mo) and Pb in 3M HNO₃ leachates, relative to corresponding carbonate
455 phases, are most likely best explained by the presence of sulfide minerals and/or organic
456 compounds in studied carbonate samples. The relative partitioning of these elements between
457 sulfide and organic phases will be discussed below.

458

459 *4.3. Trace elements in residual detrital fractions*

460 The residual detrital fractions associated with studied carbonate samples mostly correspond to
461 terrigenous silicate minerals, but also presumably include some refractory organic compounds
462 and/or sulfide minerals that were left behind after the 5% H₂O₂ and 3M HNO₃ leaching steps. In
463 this regard, the most striking feature of the dataset for detrital fractions is the pronounced
464 enrichments in Mo that characterized many samples (Fig. 2c).

465

466 In recent years, the distribution of Mo in bulk sediments at cold seeps has received increasing
467 attention, as a potential tracer of methane seepage dynamics (Peketi et al., 2012; Sato et al., 2012;
468 Hu et al., 2015b, Chen et al., 2016). The range of Mo concentrations measured in seep-related
469 sediments from the Nankai Trough (Sato et al., 2012) and the South China Sea (Chen et al., 2016)
470 is similar (up to ~32 mg/kg) to that found in the detrital fractions analyzed in this study (up to 25

471 mg/kg), being enriched by a factor of about 30 compared to other typical hemipelagic sediments
472 (Sato et al., 2012). This strong Mo enrichment was taken as an evidence that cold seep sediments
473 could possibly represent a net sink in the global biogeochemical marine cycling of Mo (Sato et al.,
474 2012; Hu et al., 2015b). Previous studies have suggested that the enrichment of Mo in marine
475 sediments could relate to high organic contents (Wilde et al., 2004; Guo et al., 2007), or to the
476 presence of high dissolved sulfide (HS^-) concentrations in the sediment, which can lead to
477 conversion of soluble molybdate (MoO_4^{2-}) into particle-reactive thiomolybdate ($\text{MoO}_x\text{S}_{4-x}^{2-}$)
478 species that are then sequestered within the sediment (Helz et al., 1996; 2011). Clearly, the
479 observed Mo enrichment in the residual silicate fractions associated with seep carbonates can be
480 ascribed to the presence of high dissolved sulfide contents at cold seeps and precipitation of
481 sulfide minerals in the sediment.

482

483 Interestingly, we did not identify any particular enrichment for tungsten (W) in studied detrital
484 fractions. Tungsten is the geochemical twin of Mo, and apart from a few differences, both
485 elements generally behave similarly in the marine environment (see Dellwig et al., 2019 for a
486 recent detailed review). In open ocean waters, both Mo and W are intensively scavenged onto
487 Fe-Mn oxyhydroxide phases, which can then be released subsequently into pore waters, following
488 sediment deposition and diagenetic alteration under suboxic/anoxic conditions. Similar to Mo,
489 high sulfide concentrations in pore waters lead to the conversion of tungstate to thiotungstate that
490 can be incorporated into Fe-sulfides or organic compounds. As will be discussed below, the
491 absence of any W enrichment in studied sulfide and detrital fractions, in contrast to Mo, suggests
492 that an unknown mechanism leads to decoupling of Mo and W in cold seep sediments.

493

494 *4.4. The characteristics of lipid biomarkers and trace elements in organic fractions*

495 The distribution patterns of microbial lipids extracted from our series of authigenic carbonate
496 samples were examined by PCA (Fig. 6). For archaeal lipids, the first PC component (PC1)
497 accounted for 42.0 % of the total variance, and the second PC component (PC2) explained 30.9%
498 of the total variance. The high abundances of isoprenoid DGDs (in particular archaeol and
499 sn-2-hydroxyarchaeol) were responsible for distinguishing between samples for PC1, whereas
500 irregular tail-to-tail isoprenoids (mainly phytane and crocetane) were important for PC2 (Fig. 6a).
501 Based on the PCA results, we also performed a hierarchical clustering of principal components
502 (HCPC) to cluster samples with archaeal lipid abundances. The samples were grouped into three
503 distinct clusters, i.e. Cluster 1, Cluster 2, and Cluster 3 (Fig. 6a). The HCPC results showed that
504 each cluster was associated with distinctive abundances of archaeal lipids investigated. Cluster 3
505 was associated with the predominant isoprenoid DGDs, which are indicative of AOM-related
506 ANME-1 and -2 assemblages. Cluster 1 with phytane + crocetane is also indicative of ANME-2
507 related to AOM, but phytane contributions to these samples might be higher than those of Cluster
508 3. In contrast, Cluster 2 related to PMI, PMI-3, and sn-3-hydroxyarchaeol archaeal lipids are more
509 related to ANME-1 and 2. Among them, the presence of saturated PMI analogue may reflect the
510 growth stages (e.g. lipid biosynthesis) of these communities (Blumenberg et al., 2005; Nauhaus et
511 al., 2007). For bacterial lipids, PC1 and PC2 accounted for 54.4% and 17.3% of the total variance,
512 respectively (Fig. 6b). Most bacterial lipids (i.e. non-isoprenoid DGDs and FAs) were responsible
513 for distinguishing between samples for PC1. The compounds having the strongest influence on
514 PC2 were non-isoprenoid DGDs. Similar to archaeal lipids, bacterial lipids were also grouped into

515 three distinct clusters (Fig. 6b). Cluster 1 identifies a distinctive group characterized by high DGD
516 (If) contributions. Cluster 2 has also a higher contribution of DGD (If) compared to Cluster 3
517 characterized, with mixed lipid patterns. In this regard, Cluster 1 and 2 appear to be associated
518 with sulfate reducing bacteria inhabiting cold seep environments (e.g. Pancost et al., 2001).

519

520 Compared to leaching with hydrogen peroxide solution, lipid extraction leads to much reduced
521 carbonate dissolution, and hence is probably best suited for investigating organic-bound trace
522 element patterns in seep carbonates. Nevertheless, the two methods result in comparatively similar
523 normalized elemental distribution patterns (Fig. 3), both displaying more or less pronounced
524 enrichments in the following elements: Li, Ti, V, Co, Ni, Cu, Zn, Mo and W. Most of these
525 elements have been already previously identified in microorganism cells, in particular in
526 seep-related microbial assemblages, where they are known to be bound to specific sites of proteins
527 and enzymes (e.g. Barton et al., 2007; Glass and Orphan, 2012). Importantly, this suggests that the
528 determination of trace element patterns in seep carbonates can provide interesting information of
529 the utility of metals to microbial life, and possibly help identifying particular elements with a
530 previously unrecognized importance for microbial metabolism at cold seeps. Microbial
531 metalloenzymes play key roles in catalyzing major biogeochemical reactions, in particular the
532 anaerobic oxidation of methane (Zerkle et al., 2005). The AOM can be largely regarded as a
533 reverse methanogenesis pathway (Hallam et al., 2004; Thauer, 2008; Scheller et al., 2010), and
534 both reactions are thought to require the same combination of trace metals ranging from Fe, Ni,
535 Co, Mo (and/or W) and Zn (Glass and Orphan, 2012). Below, we use our findings on the
536 distribution of trace elements in lipid fractions to further discuss the role of specific metals in
537 microbial methane cycling at cold seeps. In particular, by comparing lipid-bound data with
538 elemental abundances measured in corresponding carbonate and sulfide phases, we can discuss
539 how microbial activity at cold seeps can be affected by trace metal bioavailability in pore waters.

540

541 4.4.1. Ni and Co

542 Both Ni and Co are known to play a crucial role in methanogenesis and anaerobic methanotrophy
543 (e.g. Glass et al., 2012). At submarine methane seeps, Ni-containing proteins were first extracted
544 from microbial mats collected in the Black Sea, which provided one of the first direct evidence for
545 the importance of Ni in the AOM process (Krüger et al., 2003). Various geochemical
546 investigations of methanogenic archaea also revealed significant enrichments of Ni and Co at the
547 cell-scale (Cameron et al., 2012; Glass et al., 2018). A study conducted on Cretaceous
548 methane-derived carbonates identified relatively high Ni signals using laser ablation ICP-MS,
549 which were taken as evidence for past microbial activity (Reitner et al., 2015). To date, at least
550 three Ni-dependent enzymes have been identified in methanogens, including the carbon monoxide
551 dehydrogenase/acetyl-CoA (coenzyme A) synthase, and the Ni cofactor F430 in the methyl
552 coenzyme M reductase, which catalyzes the final step of methanogenesis (Ferry, 1993; Ragsdale
553 and Kumar, 1996). Cobalt is a core element of vitamin B12 (cobalamin) that can be
554 biosynthesized anaerobically by methanogens and sulfate-reducing bacteria, and is involved in
555 methanogenesis and reverse methanogenesis pathways (Glass et al., 2014). In this study, while we
556 did not find any strong relationships between lipid biomarker patterns and elemental
557 concentrations, the abundance of Co in extracted lipid fractions displays positive correlation with
558 C17:0, C18:1w9c and DGD (If). In addition, the slight positive correlations observed between

559 Ni and Co enrichments in lipid fractions (relative to 3M HNO₃ data) and our PCA results for
560 archaeal lipids (PC1 score; archaeol and *sn*-2-hydroxyarchaeol concentrations) adds further
561 support that measured lipid-bound Ni and Co abundances are related to the presence of archaeal
562 communities (Fig. 7). Importantly, the availability of Ni and Co in natural ecosystems most likely
563 represents a limiting factor for the activity of these archaeal communities (Basiliko and Yavitt,
564 2001). In this study, the evidence that studied carbonate phases always display relatively high Ni
565 and Co concentrations (Fig. 2) suggests that these elements are generally present in relative
566 abundance in surrounding pore waters. This would indicate that dissolved Ni and Co supply at
567 cold seeps (at least in those investigated during the course of this study) does not represent a
568 limiting factor on microbial activity.

569

570 4.4.2. Cu

571 While the potential utility of Cu in the anaerobic oxidation of methane is yet to be fully
572 understood (Sushkevich et al., 2017), it is well known that Cu plays a central role in the
573 metabolism of aerobic methane-oxidizing bacteria. In presence of Cu, the particulate methane
574 mono-oxygenase (pMMO), a membrane protein found in methanotrophic bacteria, catalyzes the
575 oxidation of methane to methanol. An increase in Cu concentration can result in up to 55-fold
576 expression of pMMO (Glass and Orphan, 2012). In this study, while lipid-bound Cu
577 concentrations in seep carbonates do not appear to correlate with lipid biomarker patterns, a few
578 aragonite-rich seep carbonates (sample 2-3, 2-4, with Sr/Ca > 0.020) appear to host microbial lipid
579 fractions characterized by higher Cu contents (as inferred from Cu/Ca ratios; Fig. 5). As already
580 mentioned above, aragonite precipitation at cold seeps is favored at sites characterized by high
581 methane fluxes, where the SMTZ is located at shallower sediment depth, in the near-seafloor
582 environment (e.g., Burton, 1993; Bayon et al, 2007; Peckmann et al, 2009; Nöthen and Kasten,
583 2011). Near the sediment-water interface, it is likely that methane oxidation partly proceeds
584 through Cu-dependent aerobic methane-oxidizing bacteria, which would possibly explain why
585 lipid fractions extracted from a few aragonite-rich carbonates display higher Cu contents than
586 those recovered from high-Mg carbonate phases (which presumably formed from deeper and fully
587 anoxic sediment layers). This would be in full agreement with previous biomarker investigations,
588 which also identified the presence of aerobic methanotrophs in seep carbonates formed near the
589 seafloor (Himmler et al., 2015).

590

591 4.4.3. Mo and W

592 Molybdenum (Mo) and its geochemical twin tungsten (W) are also important metals in the
593 metabolism of microbial communities involved in the AOM, especially when it is coupled to
594 nitrate reduction (Haroon et al., 2013; Glass et al., 2014). The most well-known biological
595 function for Mo is as nitrate reductase and nitrogenase enzyme (Kisker et al., 1997; Zerkle et al.,
596 2005; Glass and Orphan, 2012; Mcglynn et al., 2013), in which Mo (or W) is bound to a pterin
597 cofactor to form molybdopterin (or tungstopterin). Some methanogens also require Mo and/or W
598 in formyl-methanofuran dehydrogenases system, which catalyze the initial conversion of carbon
599 dioxide to methane (Lvov et al., 2002; Ferry, 2010).

600

601 In this study, Mo and W were found to be significantly enriched in lipid fractions, although no
602 major correlation could be identified between lipid-bound Mo-W trace element data and our PCA

603 results for archaeal lipids (figure not shown here). The ubiquitous presence of Mo in all studied
604 fractions, including lipids but also corresponding carbonate and sulfide mineral phases, indicates
605 the abundance of bioavailable Mo at cold seeps. In contrast, while W also display pronounced
606 enrichments in lipid-bound fractions, the low W concentrations determined in both carbonate
607 phases and sulfide minerals at seeps suggest instead that dissolved W concentrations in
608 surrounding pore waters are relatively depleted. While this assumption agrees with a previous
609 trace metal investigation of pore waters at Hydrate Ridge (Glass et al., 2014), which reported very
610 low dissolved W concentrations at methane seeps, it is in contrast with the fact that thiotungstate
611 should be more soluble than thiomolybdate species in pore waters (Mohajerin et al., 2014; 2016).
612 Based on the above, we speculate that the low W abundances in seep carbonate and sulfide phases
613 (and presumably in pore waters) reflect substantial microbial requirements in W during the AOM.
614 This hypothesis would be supported by previous evidence of striking correlations between W
615 enrichments and the presence of hyperthermophiles in hydrothermal mineral deposits (Holden and
616 Adams, 2003), suggesting that W may be preferred over Mo by anaerobic microbial communities
617 at submarine methane seeps (L'vov et al., 2002; Holden and Adams, 2003).

618
619

620 **5. Conclusions**

621 Our combined investigation of trace element systematics in authigenic carbonates and associated
622 lipid fractions provides evidence for the utility of trace metals to microbial life at cold seeps.
623 While trace element distribution patterns of inorganic carbonate phases mainly reflect the
624 chemical composition of surrounding pore waters at the time of carbonate precipitation,
625 pronounced trace metal enrichments associated with total lipid fractions for Ni, Co, Cu, Mo and W
626 relate to their implication in various microbial enzymatic activities.

627

628 The abundance of Ni, Co and Mo is ubiquitous in studied lipid biomarkers, but also in
629 corresponding carbonate phases and sulfide minerals, suggesting that a substantial pool of
630 dissolved Ni, Co and Mo is available at cold seeps for the microorganisms involved in the
631 anaerobic oxidation of methane. In contrast, we propose that important microbial requirement in
632 W during the AOM can lead to strong depletion of dissolved W in pore waters at cold seeps, as
633 inferred from the very low W concentrations determined in both carbonate phases and sulfide
634 minerals. This finding suggests that W could represent a limiting factor for microbial methane
635 oxidation at seeps. Overall, this study demonstrates the utility of combining trace element
636 systematics to lipid biomarker investigations in order to improve our understanding of the
637 microbial biogeochemistry of deep-sea extreme environments.

638
639

640 **Acknowledgments**

641 This project was funded by IFREMER; the National Research Foundation of Korea (NRF) grants
642 funded by the Ministry of Science and ICT (MSIT) – South Korea [NRF-2016R1A2B3015388,
643 KOPRI-PN19100 and NRF-2015M1A5A1037243, KOPRI-PN19090]; and the National Key
644 R&D Program of China (2018YFC0310003), the National Program on Global Change and Air-Sea
645 Interaction (GASI-GEOGE-05-04), and the NSF of China (Grants: 41773091, 41730528, and
646 41761134084). We thank H.H. Roberts for providing the Gulf of Mexico seep carbonate samples.

647 Xudong Wang acknowledges the China Scholarship Council for supporting a research visit to
648 IFREMER.

649

650

651 **References**

652 Aloisi, G., Pierre, C., Rouchy, J.M., Foucher, J.P., Woodside, J., the MEDINAUT Scientific Party,
653 2000. Methane-related authigenic carbonates of eastern Mediterranean Sea mud volcanoes and
654 their possible relation to gas hydrate destabilisation. *Earth Planet. Sci. Lett.* 184, 321–338.

655

656 Aloisi, G., Bouloubassi, I., Heijs, S.K., Pancost, R.D., Pierre, C., Sinninghe Damsté, J.P., Gottschal,
657 J.C., Forney, L.J., Rouchy, J.-M., 2002. CH₄-consuming microorganisms and the formation of
658 carbonate crusts at cold seeps. *Earth Planet. Sci. Lett.* 203, 195–203.

659

660 Anbar, A.D., 2008. Elements and Evolution. *Science* 322, 1481–1483.

661

662 Barrat, J.A., Keller, F., Amossé, J., Taylor, R.N., Nesbitt, R.W., Hirata, T., 1996. Determination of
663 rare earth elements in sixteen silicate reference samples by ICP-MS after Tm addition and
664 ion-exchange separation. *Geostand. Geoanal. Res.* 20, 133–139.

665

666 Barrat, J.A., Zanda, B., Moynier, F., Bollinger, C., Liorzou, C., Bayon, G., 2012. Geochemistry of
667 CI chondrites: Major and trace elements, and Cu and Zn Isotopes. *Geochim. Cosmochim. Acta* 83,
668 79–92.

669

670 Barton, L.L., Goulhen, F., Bruschi, M., Woodards, N.A., Plunkett, R.M., Rietmeijer, F.J.M., 2007.
671 The bacterial metallome: composition and stability with specific reference to the anaerobic
672 bacterium *Desulfovibrio desulfuricans*. *Biometals* 20, 291–302.

673

674 Basiliko, N., Yavitt, J.B., 2001. Influence of Ni, Co, Fe, and Na additions on methane production
675 in Sphagnum-dominated Northern American peatlands. *Biogeochemistry* 52, 133–153.

676

677 Bayon, G., German, C.R., Boella, R.M., Milton, J.A., Taylor, R.N., Nesbitt, R.W., 2002. An
678 improved method for extracting marine sediment fractions and its application to Sr and Nd
679 isotopic analysis. *Chem. Geol.* 187, 179–199.

680

681 Bayon, G., Pierre, C., Etoubleau, J., Voisset, M., Cauquil, E., Marsset, T., Sultan, N., Le Drezen,
682 E., Fouquet, Y., 2007. Sr/Ca and Mg/Ca ratios in Niger Delta sediments: implications for
683 authigenic carbonate genesis in cold seep environments. *Mar. Geol.* 241, 93–109.

684

685 Bayon, G., Barrat, J.A., Etoubleau, J., Benoit, M., Bollinger, C., Révillon, S., 2009. Determination
686 of rare earth elements, Sc, Y, Zr, Ba, Hf and Th in geological samples by ICP-MS after Tm
687 addition and alkaline fusion. *Geostand. Geoanal. Res.* 33, 51–62.

688

689 Bayon, G., Birot, D., Ruffine, L., Caprais, J.-C., Ponzevera, E., Bollinger, C., Donval, J.-P.,
690 Charlou, J.-L., Voisset, M., Grimaud, S., 2011a. Evidence for intense REE scavenging at cold

691 seeps from the Niger Delta margin. *Earth Planet. Sci. Lett.* 312, 443–452.
692
693 Bayon, G., Birot, D., Bollinger, C., Barrat, J-A., 2011b. Multi-Element Determination of Trace
694 Elements in Natural Water Reference Materials by ICP-SFMS after Tm Addition and Iron
695 Co-precipitation. *Geostand. Geoanal. Res.* 35, 145–153.
696
697 Bayon, G., Toucanne, S., Skonieczny, C., André, L., Bermell, S., Cheron, S., Dennielou, B.,
698 Etoubleau, J., Freslon, N., Gauchery, T., Germain, Y., Jorry, S.J., Ménot, G., Monin, L., Ponzevera,
699 E., Rouget, M.-L., Tachikawa, K., Barrat, J.A., 2015. Rare earth elements and neodymium
700 isotopes in world river sediments revisited. *Geochim. Cosmochim. Acta* 170, 17–38.
701
702 Beal, E.J., House, C.H., Orphan, V.J., 2009. Manganese- and Iron-Dependent Marine Methane
703 Oxidation. *Science* 325, 184–187.
704
705 Blumenberg, M., Seifert, R., Nauhaus, K., Pape, T., Michaelis, W., 2005. In Vitro Study of Lipid
706 Biosynthesis in an Anaerobically Methane-Oxidizing Microbial Mat. *Appl. Environ. Microbiol.* 71,
707 4345–4351.
708
709 Boetius, A., Ravensschlag, K., Schubert, C.J., Rickert, D., Widdel, F., Gieseke, A., Amann, R.,
710 Jørgensen, B.B., Witte, U., Pfannkuche, O., 2000. A marine microbial consortium apparently
711 mediating anaerobic oxidation of methane. *Nature* 407, 623–626.
712
713 Burton, E.A., 1993. Controls on marine carbonate cement mineralogy: review and reassessment.
714 *Chem. Geol.* 105, 163–179.
715
716 Cameron, V., House, C.H., Brantley, S.L., 2012. A First Analysis of Metallome Biosignatures of
717 Hyperthermophilic Archaea. *Archaea*, 1–12.
718
719 Cangemi, M., Leonardo, R.D., Bellanca, A., Cundy, A., Neri, R., Angelone, M., 2010.
720 Geochemistry and mineralogy of sediments and authigenic carbonates from the Malta Plateau,
721 Strait of Sicily (Central Mediterranean): Relationships with mud/fluid release from a mud volcano
722 system. *Chem. Geol.* 276, 294–308.
723
724 Chao, T.T., Sanzolone, R.F., 1977. Chemical dissolution of sulfide minerals. *Journal of Research*
725 *of the U.S. Geological Survey* 5, 409–412.
726
727 Chen, F., Hu, Y., Feng, D., Zhang, X., Cheng, S., Cao, J., Lu, H., Chen D., 2016. Evidence of
728 intense methane seepages from molybdenum enrichments in gas hydrate-bearing sediments of the
729 northern South China Sea. *Chem. Geol.* 443, 173–181.
730
731 Conti, S., Fontana, D., Gubertini, A., Sighinolfi, G., Tateo, F., Fioroni, C., Fregni, P., 2004. A
732 multidisciplinary study of middle Miocene seep-carbonates from the northern Apennine foredeep
733 (Italy). *Sediment. Geol.* 169, 1–19.
734

735 Dellwig, O., Wegwerth, A., Schnetger, B., Schulz, H., Arz, H.W., 2019. Dissimilar behaviors of
736 the geochemical twins W and Mo in hypoxic-euxinic marine basins. *Earth-Sci. Rev.* 193, 1–23.
737

738 Dold, B., 2003. Speciation of the most soluble phases in a sequential extraction procedure adapted
739 for geochemical studies of copper sulfide mine waste. *J. Geochem. Explor.* 80, 55–68.
740

741 Feng, D., Chen, D., Peckmann, J., 2009. Rare earth elements in seep carbonates as tracers of
742 variable redox conditions at ancient hydrocarbon seeps. *Terr. Nova* 21, 49–56.
743

744 Feng, D., Roberts, H.H., 2010. Initial results of comparing cold-seep carbonates from mussel- and
745 tubeworm-associated environments at Atwater Valley lease block 340, northern Gulf of Mexico.
746 *Deep-Sea Res. Part II-Top. Stud. Oceanogr.* 57, 2030–2039.
747

748 Feng, D., Roberts, H.H., 2011. Geochemical characteristics of the barite deposits at cold seeps
749 from the northern Gulf of Mexico continental slope. *Earth Planet. Sci. Lett.* 309, 89–99.
750

751 Feng, D., Chen, D., 2015. Authigenic carbonates from an active cold seep of the northern South
752 China Sea: new insights into fluid sources and past seepage activity. *Deep-Sea Res. Part II-Top.*
753 *Stud. Oceanogr.* 122, 74–83.
754

755 Ferry, J.G., 1993. *Methanogenesis: Ecology, Physiology, Biochemistry & Genetics*, Chapman &
756 Hall, New York, NY, USA.
757

758 Ferry, J.G., 2010. How to make a living by exhaling methane. *Annu. Rev. Microbiol.* 64, 453–473.
759

760 Freslon, N., Bayon, G., Birot, D., Bollinger, C., Barrat, J.A., 2011. Determination of rare earth
761 elements and other trace elements (Y, Mn, Co, Cr) in seawater using Tm addition and Mg(OH)₂
762 co-precipitation. *Talanta* 85, 582–587.
763

764 Freslon, N., Bayon, G., Toucanne, S., Bermell, S., Bollinger, C., Chéron, S., Etoubleau, J.,
765 Germain, Y., Khripounoff, A., Ponzevera, E., Rouget, M.L., 2014. Rare earth elements and
766 neodymium isotopes in sedimentary organic matter. *Geochim. Cosmochim. Acta* 140, 177–198.
767

768 Frimmel, H.E., 2009. Trace element distribution in Neoproterozoic carbonates as
769 palaeoenvironmental indicator. *Chem. Geol.* 258, 338–353.
770

771 Ge, L., Jiang, S., Swennen, R., Yang, T., Yang, J., Wu, N., Liu, J., Chen D., 2010. Chemical
772 environment of cold seep carbonate formation on the northern continental slope of South China
773 Sea: Evidence from trace and rare earth element geochemistry. *Mar. Geol.* 277, 21–30.
774

775 Ge, L., Jiang, S., 2013. Sr isotopic compositions of cold seep carbonates from the South China Sea
776 and the Panoche Hills (California, USA) and their significance in palaeoceanography. *J. Asian*
777 *Earth Sci.* 65, 34–41.
778

779 Glass, J.B., Orphan, V.J., 2012. Trace Metal Requirements for Microbial Enzymes Involved in the
780 Production and Consumption of Methane and Nitrous Oxide. *Front. Microbiol.* 3, 61.
781 doi:10.3389/fmicb.2012.00061.
782

783 Glass, J.B., Yu, H., Steele, J.A., Dawson, K.S., Sun, S., Chourey, K., Pan, C., Hettich, R.L.,
784 Orphan, V.J., 2014. Geochemical, metagenomic and metaproteomic insights into trace metal
785 utilization by methane-oxidizing microbial consortia in sulphidic marine sediments. *Environ.*
786 *Microbiol.* 16, 1592–1611.
787

788 Glass, J.B., Chen, S., Dawson, K.S., Horton, D.R., Vogt, S., Ingall, E.D., Twining, B.S., Orphan,
789 V.J., 2018. Trace Metal Imaging of Sulfate-Reducing Bacteria and Methanogenic Archaea at
790 Single-Cell Resolution by Synchrotron X-Ray Fluorescence Imaging. *Geomicrobiol. J.* 1-9, doi:
791 10.1080/01490451.2017.1321068.
792

793 Guan, H., Feng, D., Wu, N., Chen, D., 2016. Methane seepage intensities traced by biomarker
794 patterns in authigenic carbonates from the South China Sea. *Org. Geochem.* 91, 109–119.
795

796 Guo, Q., Shields, G.A., Liu, C., Strauss, H., Zhu, M., Pi, D., Goldberg, T., Yang, X., 2007. Trace
797 element chemostratigraphy of two Ediacaran–Cambrian successions in south China: Implications
798 for organosedimentary metal enrichment and silicification in the Early Cambrian. *Palaeogeogr.*
799 *Palaeoclimatol. Palaeoecol.* 254, 194–216.
800

801 Haley, B.A., Klinkhammer, G.P., Mcmanus, J., 2004. Rare earth elements in pore waters of marine
802 sediments. *Geochim. Cosmochim. Acta* 68, 1265–1279.
803

804 Hallam, S.J., Putman, N., Preston, C.M., Detter, J.C., Rokhsar, D., Richardson, P.M., DeLong, E.F.,
805 2004. Reverse methanogenesis: testing the hypothesis with environmental genomics. *Science* 305,
806 1457–1462.
807

808 Haroon, M.F., Hu, S., Shi, Y., Imelfort, M., Keller, J., Hugenholtz, P., Yuan, Z., Tyson, G.W., 2013.
809 Anaerobic oxidation of methane coupled to nitrate reduction in a novel archaeal lineage. *Nature*
810 500, 567–570.
811

812 Helz, G.R., Miller, C.V., Charnock, J.M., Mosselmans, J.F.W., Patrick, R.A.D., Garner, C.D.,
813 Vaughan, D.J., 1996. Mechanism of molybdenum removal from the sea and its concentration in
814 black shales: EXAFS evidence. *Geochim. Cosmochim. Acta* 60, 3631–3642.
815

816 Helz, G.R., Bura-Nakić, E., Mikac, N., Ciglenc̆ki, I., 2011. New model for molybdenum behavior
817 in euxinic waters. *Chem. Geol.* 284, 323–332.
818

819 Himmler, T., Bach, W., Bohrmann, G., Peckmann, J., 2010. Rare earth elements in authigenic
820 methane-seep carbonates as tracers for fluid composition during early diagenesis. *Chem. Geol.*
821 277, 126–136.
822

823 Himmler, T., Birgel, D., Bayon, G., Pape, T., Ge, L., Bohrmann, G., Peckmann, J., 2015.
824 Formation of seep carbonates along the Makran convergent margin, northern Arabian Sea and a
825 molecular and isotopic approach to constrain the carbon isotopic composition of parent methane.
826 *Chem. Geol.* 415, 102–117.
827

828 Holden, J.F., Adams, M.W.W., 2003. Microbe-metal interactions in marine hydrothermal
829 environments. *Curr. Opin. Chem. Biol.* 7, 160–165.
830

831 Hu, Y., Feng, D., Peckmann, J., Roberts, H.H., Chen, D., 2014. New insights into cerium
832 anomalies and mechanisms of trace metal enrichment in authigenic carbonate from hydrocarbon
833 seeps. *Chem. Geol.* 381, 55–66.
834

835 Hu, Y., Feng, D., Chen, L., Zheng, G., Peckmann, J., Chen, D., 2015a. Using iron speciation in
836 authigenic carbonates from hydrocarbon seeps to trace variable redox conditions. *Mar. Pet. Geol.*
837 67, 111–119.
838

839 Hu, Y., Feng, D., Liang, Q., Xia, Z., Chen, L., Chen, D., 2015b. Impact of anaerobic oxidation of
840 methane on the geochemical cycle of redox-sensitive elements at cold-seep sites of the northern
841 South China Sea. *Deep-Sea Res. Part II-Top. Stud. Oceanogr.* 122, 84–94.
842

843 Jahn, B., Pol, A., Lumpe, H., Barends, T.R.M., Dietl, A., Hogendoorn, C., Op den Camp, H.J.M.,
844 Daumann, L.J., 2018. Similar but Not the Same: First Kinetic and Structural Analyses of a
845 Methanol Dehydrogenase Containing a Europium Ion in the Active Site. *ChemBioChem*, doi:
846 10.1002/cbic.201800130.
847

848 Jochum, K.P., Weis, U., Schwager, B., Stoll, B., Wilson, S.A., Haug, G.H., Andreae, M.O.,
849 Enzweiler, J., 2016. Reference Values Following ISO Guidelines for Frequently Requested Rock
850 Reference Materials. *Geostand. Geoanal. Res.* 40, 333–350.
851

852 Jørgensen, N.O., 1992. Methane-derived carbonate cementation of marine sediments from the
853 Kattegat, Denmark: Geochemical and geological evidence. *Mar. Geol.* 103, 1–13.
854

855 Joye, S.B., Boetius, A., Orcutt, B.N., Montoya, J.P., Schulz, H.N., Erickson, M.J., Lugo, S.K.,
856 2004. The anaerobic oxidation of methane and sulfate reduction in sediments from Gulf of Mexico
857 cold seeps. *Chem. Geol.* 205, 219–238.
858

859 Kisker, C., Schindelin, H., Rees, D.C., 1997. Molybdenum-cofactor-containing enzymes: structure
860 and mechanism. *Annu. Rev. Biochem.* 66, 233–267.
861

862 Konhauser, K.O., Pecoits, E., Lalonde, S.V., Papineau, D., Nisbet, E.G., Barley, M.E., Arndt, N.T.,
863 Zahnle, K., Kamber, B.S., 2009. Oceanic nickel depletion and a methanogen famine before the
864 great oxidation event. *Nature* 458, 750–753.
865

866 Krüger, M., Meyerdierks, A., Glockner, F.O., Amann, R., Widdel, F., Kube, M., Reinhardt, R.,

867 Kahnt, J., Böcher, R., Thauer, R.K., Shima, S., 2003. A conspicuous nickel protein in microbial
868 mats that oxidize methane anaerobically. *Nature* 426, 878–881
869

870 Lee, D.H., Kim, J.H., Lee, Y.M., Stadnitskaia, A., Jin, Y.K., Niemann, H., Kim, Y.G., Shin, K.H.,
871 2018. Biogeochemical evidence of anaerobic methane oxidation on active submarine mud
872 volcanoes on the continental slope of the Canadian Beaufort Sea. *Biogeosciences*, 15, 7419–7433.
873

874 Lemaitre, N., Bayon, G., Ondréas, H., Caprais, J.C., Freslon, N., Bollinger, C., Rouget, M.L., de
875 Prunelé, A., Ruffine, L., Roy, K.O.L., Sarthou, G., 2014. Trace element behaviour at cold seeps
876 and the potential export of dissolved iron to the ocean. *Earth Planet. Sci. Lett.* 404, 376–388.
877

878 Levin, L.A., 2005. Ecology of cold seep sediments: Interactions of fauna with flow, chemistry and
879 microbes. *Oceanogr. Mar. Biol.* 43, 1–46.
880

881 Liang, Q., Hu, Y., Feng, D., Peckmann, J., Chen, L., Yang, S., Liang, J., Tao, J., Chen, D., 2017.
882 Authigenic carbonates from newly discovered active cold seeps on the northwestern slope of the
883 South China Sea: Constraints on fluid sources, formation environments, and seepage dynamics.
884 *Deep-Sea Res. Part I-Oceanogr. Res. Pap.* 124, 31–41.
885

886 Lu, Y., Liu, Y., Sun, X., Lin, Z., Xu, L., Lu, H., Hao, X., Peckmann, J., 2017. Intensity of methane
887 seepage reflected by relative enrichment of heavy magnesium isotopes in authigenic carbonates: A
888 case study from the South China Sea. *Deep-Sea Res. Part I-Oceanogr. Res. Pap.* 129, 10–21.
889

890 Luff, R., Wallmann, K., 2003. Fluid flow, methane fluxes, carbonate precipitation and
891 biogeochemical turnover in gas hydrate-bearing sediments at Hydrate Ridge, Cascadia Margin:
892 numerical modeling and mass balances. *Geochim. Cosmochim. Acta* 67, 3403–3421.
893

894 L'vov, N. P., Nosikov, A. N., Antipov, A. N., 2002. Tungsten-containing enzymes.
895 *Biochem.-Moscow* 67, 196–200.
896

897 Mcglynn, S.E., Boyd, E.S., Peters, J.W., Orphan, V.J., 2013. Classifying the metal dependence of
898 uncharacterized nitrogenases. *Front. Microbiol.* 3, 1–8.
899

900 Michaelis, W., Seifert, R., Nauhaus, K., Treude, T., Thiel, V., Blumenberg, M., Knittel, K., Gieseke,
901 A., Peterknecht, K., Pape, T., Boetius, A., Amann, R., Jørgensen, B.B., Widdel, F., Peckmann, J.,
902 Pimenov, N.V., Gulin, M.B. 2002. Microbial Reefs in the Black Sea Fueled by Anaerobic
903 Oxidation of Methane. *Science* 297, 1013–1015.
904

905 Mohajerin, T.J., Helz, G.R., White, C.D., Johannesson, K.H., 2014. Tungsten speciation in sulfidic
906 waters: Determination of thiotungstate formation constants and modeling their distribution in
907 natural waters. *Geochim. Cosmochim. Acta* 144:157–172.
908

909 Mohajerin, T.J., Helz, G.R., Johannesson, K.H., 2016. Tungsten–molybdenum fractionation in
910 estuarine environments. *Geochim. Cosmochim. Acta* 177, 105–119.

911
912 Morford, J.L., Emerson, S., 1999. The geochemistry of redox sensitive trace metals in sediments.
913 *Geochim. Cosmochim. Acta* 63, 1735–1750.
914
915 Nance, W.B., Taylor, S.R., 1976. Rare earth element patterns and crustal evolution—I. Australian
916 post-Archean sedimentary rocks. *Geochim. Cosmochim. Acta* 40, 1539–1551.
917
918 Nauhaus, K., Albrecht, M., Elvert, M., Boetius, A., Widdel, F., 2007. In vitro cell growth of marine
919 archaeal-bacterial consortia during anaerobic oxidation of methane with sulfate. *Environ.*
920 *Microbiol.* 9, 187–196.
921
922 Nothdurft, L.D., Webb, G.E., Kamber, B.S., 2004. Rare earth element geochemistry of Late
923 Devonian reefal carbonates, Canning Basin, western Australia: confirmation of a seawater REE
924 proxy in ancient limestones. *Geochim. Cosmochim. Acta* 68, 263–283.
925
926 Nöthen, K., Kasten, S., 2011. Reconstructing changes in seep activity by means of pore water and
927 solid phase Sr/Ca and Mg/Ca ratios in pockmark sediments of the northern Congo Fan. *Mar. Geol.*
928 287, 1–13.
929
930 Pancost, R.D., Bouloubassi, I., Aloisi, G., Damsté, J.S.S., the Medinaut Shipboard Scientific Party,
931 2001. Three series of non-isoprenoidal dialkyl glycerol diethers in cold-seep carbonate crusts. *Org.*
932 *Geochem.* 32, 695–707
933
934 Peckmann, J., Reimer, A., Luth, U., Luth, C., Hansen, B., Heinicke, C., Hoefs, J., Reitner, J., 2001.
935 Methane-derived carbonates and authigenic pyrite from the northwestern Black Sea. *Mar. Geol.*
936 177, 129–150.
937
938 Peckmann, J., Birgel, D., Kiel, S., 2009. Molecular fossils reveal fluid composition and flow
939 intensity at a Cretaceous seep. *Geology* 37, 847–850.
940
941 Peketi, A., Mazumdar, A., Joshi, R.K., Patil, D.J., Srinivas, P.L., Dayal, A.M., 2012. Tracing the
942 Paleo sulfate-methane transition zones and H₂S seepage events in marine sediments: An
943 application of C-S-Mo systematics. *Geochem. Geophys. Geosyst.* 13, Q10007,
944 doi:10.1029/2012GC004288.
945
946 Picone, N., Op den Camp, H.J.M., 2019. Role of rare earth elements in methanol oxidation. *Curr.*
947 *Opin. Chem. Biol.* 49, 39–44.
948
949 Pierre, C., Fouquet, Y., 2007. Authigenic carbonates from methane seeps of the Congo deep-sea
950 fan. *Geo-Mar. Lett.* 27, 249–257.
951
952 Pingitore Jr, N.E., Eastman, M.P., 1984. The experimental partitioning of Ba²⁺ into calcite. *Chem.*
953 *Geol.* 45, 113–120.
954

955 Pol, A., Barends, T.R.M., Dietl, A., Khadem, A.F., Eygensteyn, J., Jetten, M.S.M., Op den Camp,
956 H.J.M., 2014. Rare earth metals are essential for methanotrophic life in volcanic mudpots. *Environ.*
957 *Microbiol.* 16, 255–264.

958

959 Raghoebarsing, A.A., Pol, A., van de P-S, K.T., Smolders, A.J.P., Ettwig, K.F., Rijpstra, W.I.C.,
960 Schouten, S., Sinninghe Damsté, J.S., Op den Camp, H.J.M., Jetten, M.S.M., Strous, M., 2006. A
961 microbial consortium couples anaerobic methane oxidation to denitrification. *Nature* 440, 918–
962 921.

963

964 Ragsdale, S.W., Kumar, M., 1996. Nickel-Containing Carbon Monoxide
965 Dehydrogenase/Acetyl-CoA Synthase. *Chem. Rev.* 96(7), 2515–2540.

966

967 Reinhard, C.T., Lalonde, S.V., Lyons, T.W., 2013. Oxidative sulfide dissolution on the early Earth.
968 *Chem. Geol.* 362, 44–55.

969

970 Reitner, J., Blumenberg, M., Walliser, E.O., Schäfer, N., Duda, J.P., 2015. Methane-derived
971 carbonate conduits from the late Aptian of Salinac (Marne Bleues, Vocontian Basin, France):
972 Petrology and biosignatures. *Mar. Pet. Geol.* 66, 641–652.

973

974 Roberts, H.H., Feng, D., Joye, S.B., 2010. Cold-seep carbonates of the middle and lower
975 continental slope, northern Gulf of Mexico. *Deep-Sea Res. Part II-Top. Stud. Oceanogr.* 57, 2040–
976 2054.

977

978 Rongemaille, E., Bayon, G., Pierre, C., Bollinger, C., Chu, N.C., Fouquet, Y., Riboulot, V., Voisset,
979 M., 2011. Rare earth elements in cold seep carbonates from the Niger delta. *Chem. Geol.* 286,
980 196–206.

981

982 Sarkar, A., Sarangi, S., Ebihara, M., Bhattacharya, S.K., Ray, A.K., 2003. Carbonate geochemistry
983 across the Eocene/Oligocene boundary of Kutch, western India: implications to oceanic O₂-poor
984 condition and foraminiferal extinction. *Chem. Geol.* 201, 281–293.

985

986 Sato, H., Hayashi, K.I., Ogawa, Y., Kawamura, K., 2012. Geochemistry of deep sea sediments at
987 cold seep sites in the Nankai Trough: Insights into the effect of anaerobic oxidation of methane.
988 *Mar. Geol.* 323–325.

989

990 Savard, M.M., Beauchamp, B., Veizer, J., 1996. Significance of Aragonite Cements Around
991 Cretaceous Marine Methane Seeps. *J. Sediment. Res.* 66(3), 430–438.

992

993 Scheller, S., Goenrich, M., Boecher, R., Thauer, R.K., Jaun, B., 2010. The key nickel enzyme of
994 methanogenesis catalyses the anaerobic oxidation of methane. *Nature* 465, 606–608.

995

996 Scheller, S., Ermler, U., Shima, S., 2017. Catabolic Pathways and Enzymes Involved in Anaerobic
997 Methane Oxidation. *Anaerobic Utilization of Hydrocarbons, Oils, and Lipids, Handbook of*
998 *Hydrocarbon and Lipid Microbiology*, doi:10.1007/978-3-319-33598-8_3-1.

- 1000 Scherer, P., Lippert, H., Wolff, G., 1983. Composition of the major elements and trace elements of
1001 10 methanogenic bacteria determined by inductively coupled plasma emission spectrometry. *Biol.*
1002 *Trace Elem. Res.* 5, 149–163.
- 1003
- 1004 Sibuet, M., Olu, K., 1998. Biogeography, biodiversity and fluid dependence of deep-sea cold-seep
1005 communities at active and passive margins. *Deep-Sea Res. Part II-Top. Stud. Oceanogr.* 45, 517–
1006 567.
- 1007
- 1008 Snyder, G.T., Hiruta, A., Matsumoto, R., Dickens, G.R., Tomaru, H., Takeuchi, R., Komatsubara,
1009 J., Ishida, Y., Yu, H., 2007. Pore water profiles and authigenic mineralization in shallow marine
1010 sediments above the methane-charged system on Umitaka Spur, Japan Sea. *Deep-Sea Res. Part*
1011 *II-Top. Stud. Oceanogr.* 54, 1216–1239.
- 1012
- 1013 Soyol-Erdene, T.-O., Huh, Y., 2013. Rare earth element cycling in the pore waters of the Bering
1014 Sea Slope (IODP Exp. 323). *Chem. Geol.* 358, 75–89.
- 1015
- 1016 Stadnitskaia, A., Ivanov, M.K., Damsté, J.S.S., 2008. Application of lipid biomarkers to detect
1017 sources of organic matter in mud volcano deposits and post-eruptional methanotrophic processes
1018 in the Gulf of Cadiz, NE Atlantic. *Mar. Geol.* 255, 1–14.
- 1019
- 1020 Straaten, F.V.D., Schenk, V., John, T., Gao, J., 2008. Blueschist-facies rehydration of eclogites
1021 (Tian Shan, NW-China): Implications for fluid–rock interaction in the subduction channel. *Chem.*
1022 *Geol.* 255, 195–219.
- 1023
- 1024 Sun, Z., Wei, H., Zhang, X., Shang, L., Yin, X., Sun, Y., Xu, L., Huang, W., Zhang, X., 2015. A
1025 unique Fe-rich carbonate chimney associated with cold seeps in the Northern Okinawa Trough,
1026 East China Sea. *Deep-Sea Res. Part I-Oceanogr. Res. Pap.* 95, 37–53.
- 1027
- 1028 Sushkevich, V.L., Palagin, D., Ranocchiaro, M., Bokhoven J.A.van., 2017. Selective anaerobic
1029 oxidation of methane enables direct synthesis of methanol. *Science* 356, 523–527.
- 1030
- 1031 Tachikawa, K., Piotrowski, A.M., Bayon, G., 2014. Neodymium associated with foraminiferal
1032 carbonate as a recorder of seawater isotopic signatures. *Quat. Sci. Rev.* 88,1–13.
- 1033
- 1034 Taylor, S.R., McLennan, S.M., 1985. *The Continental Crust: Its Composition and Evolution. An*
1035 *Examination of the Geochemical Record Preserved in Sedimentary Rocks.* Blackwell Scientific
1036 Publications, Oxford.
- 1037
- 1038 Thauer, R.K., Shima, S., 2008. Methane as fuel for anaerobic microorganisms. *Ann. NY Acad. Sci.*
1039 1125, 158–170.
- 1040
- 1041 Thauer, R.K., Kaster, A.K., Goenrich, M., Schick, M., Hiromoto, T., Shima, S., 2010.
1042 Hydrogenases from Methanogenic Archaea, Nickel, a Novel Cofactor, and H₂ Storage. *Annu. Rev.*

1043 Biochem. 79, 507–536.
1044
1045 Torres, M.E., Mcmanus, J., Huh, C.A., 2002. Fluid seepage along the San Clemente Fault scarp:
1046 basin-wide impact on barium cycling. *Earth Planet. Sci. Lett.* 203, 181–194.
1047
1048 Torres, M.E., Martin, R.A., Klinkhammer, G.P., Nesbitt, E.A., 2010. Post depositional alteration of
1049 foraminiferal shells in cold seep settings: New insights from flow-through time-resolved analyses
1050 of biogenic and inorganic seep carbonates. *Earth Planet. Sci. Lett.* 299, 10–22.
1051
1052 Tribovillard, N., Du Châtelet, E.A., Gay, A., Barbecot, F., Sansjofre, P., Potdevin, J.L., 2013.
1053 Geochemistry of cold seepage-impacted sediments: Per-ascensum or per-descensum trace metal
1054 enrichment? *Chem. Geol.* 340, 1–12.
1055
1056 Vigneron, A., Cruaud, P., Pignet, P., Caprais, J.C., Cambon-Bonavita, M.A., Godfroy, A., Toffin L.,
1057 2013. Archaeal and anaerobic methane oxidizer communities in the Sonora Margin cold seeps,
1058 Guaymas Basin (Gulf of California). *The ISME Journal* 7,1595–1608.
1059
1060 Wang, Q., Chen, D., Peckmann, J., 2019. Iron shuttle controls on molybdenum, arsenic, and
1061 antimony enrichment in Pliocene methane-seep carbonates from the southern Western Foothills,
1062 Southwestern Taiwan. *Mar. Pet. Geol.* 100, 263–269.
1063
1064 Wilde, P., Lyons, T.W., Quinby-Hunt, M.S., 2004. Organic carbon proxies in black shales:
1065 molybdenum. *Chem. Geol.* 206, 167–176.
1066
1067 Yunker, M.B., Belicka, L.L., Harvey, H.R., Macdonald, R.W., 2005. Tracing the inputs and fate of
1068 marine and terrigenous organic matter in Arctic Ocean sediments: A multivariate analysis of lipid
1069 biomarkers. *Deep-Sea Res. Part II-Top. Stud. Oceanogr.* 52, 3478–3508.
1070
1071 Zerkle, A.L., House, C.H., Brantley, S.L., 2005. Biogeochemical signatures through time as
1072 inferred from whole microbial genomes. *Am. J. Sci.* 305, 467–502.
1073
1074

1075 **Figure captions**

1076 **Figure 1.** Global map showing the five study areas: 1) Congo fan; 2) Nile deep-sea fan; 3) Niger
1077 fan; 4) Eastern Mediterranean Sea; 5) Gulf of Mexico.
1078

1079 **Figure 2.** Enrichment factor of inorganic fractions (carbonate phases + sulfide minerals + detrital
1080 silicate fractions). (a) 1M acetic acid (AA) leachate data normalized to values for the JLs-1
1081 carbonate reference material; (b) 3M HNO₃ leachate data normalized to values for corresponding
1082 1M AA leachates; (c) conc. HF + HCl data normalized to post-Archaean Australian shale (PAAS)
1083 reference values.
1084

1085 **Figure 3.** Enrichment factor of organic fractions (organic compounds + lipid biomarkers). (a) 5%
1086 H₂O₂ leachate data normalized to values for corresponding 1M acetic acid (AA) leachates; (b) 5%

1087 H₂O₂ leachate data normalized to values for corresponding 3M HNO₃ leachates; (c) lipid-bound
1088 trace element data normalized to values for 1M AA leachates; (d) lipid-bound trace-element data
1089 normalized to values for 3M HNO₃ leachates.

1090

1091 **Figure 4.** Metal/Ca ratios in 1M acetic acid (AA) leachates. (a) Sr/Ca versus Mn/Ca; (b) Sr/Ca
1092 versus U/Ca; (c) Sr/Ca versus Ba/Ca; (d) Sr/Ca versus Nd/Ca.

1093

1094 **Figure 5.** Cu/Ca ratios in extracted lipid fractions versus Sr/Ca in corresponding 1M acetic acid
1095 (AA) leachates.

1096

1097 **Figure 6.** Principal component analysis (PCA) results for microbial lipid biomarkers. (a) archaeal
1098 and (b) bacterial compounds.

1099

1100 **Figure 7.** Results of PCA for archaeal lipids (PC1 score) versus enrichment factors for Ni and Co
1101 in carbonate-hosted lipid fractions. The slight positive correlations provide support that
1102 lipid-bound Ni and Co abundances are related to archaeal and *sn*-2-hydroxyarchaeal
1103 concentrations.

1104

1105 **Table captions**

1106 **Table 1.** Site information, water depth, mineral compositions, and carbon and oxygen stable
1107 isotopic data for the seep carbonate analyzed in this study.

1108

1109 **Table 2.** Trace element abundances (mg/kg) of certified reference materials (BHVO-2 and JLs-1).

1110

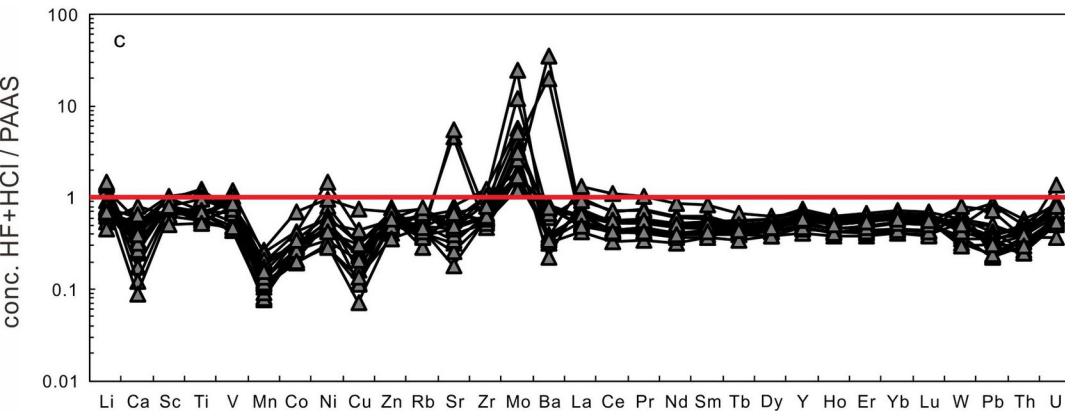
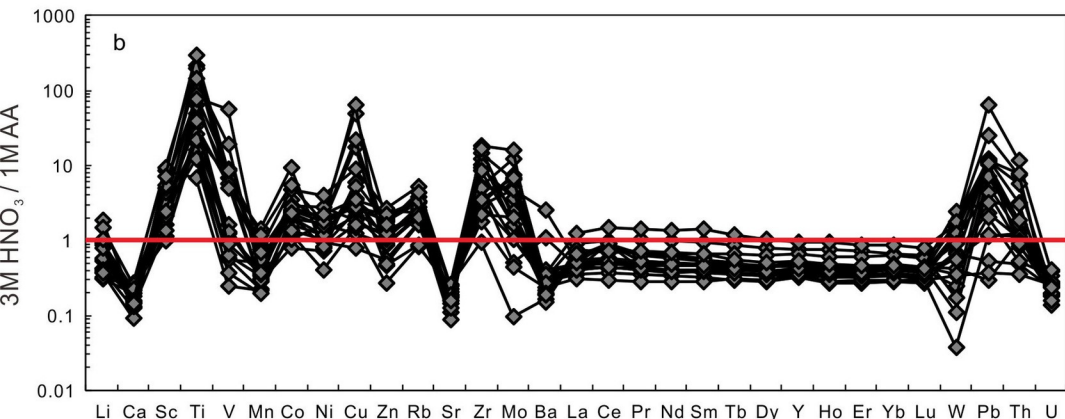
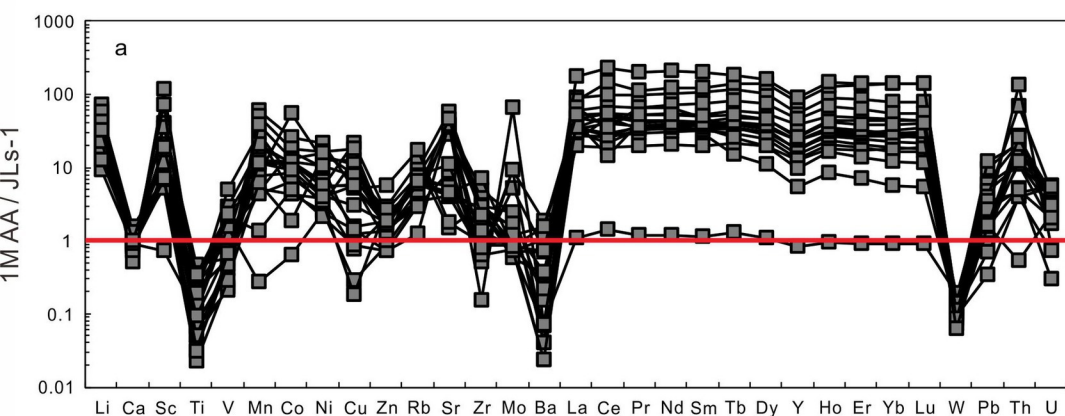
1111 **Table 3.** Element concentrations (mg/kg) of studied cold seep carbonate samples.

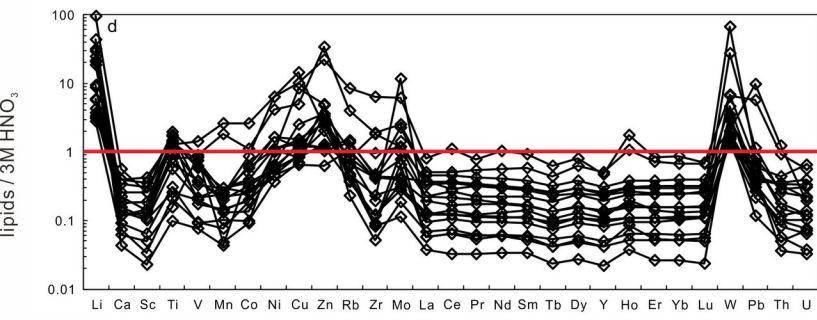
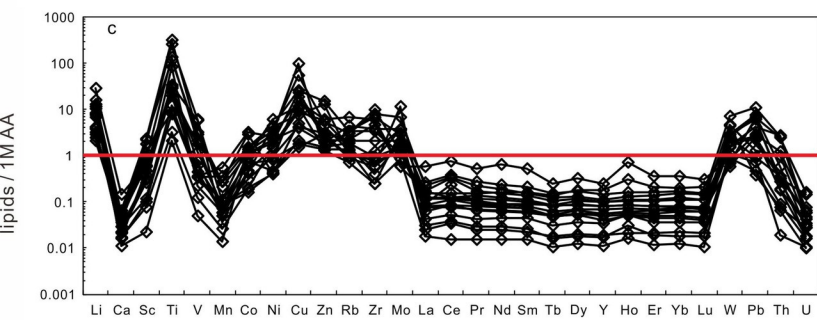
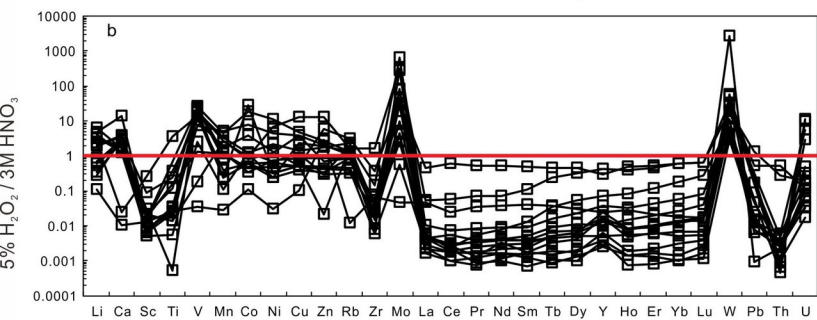
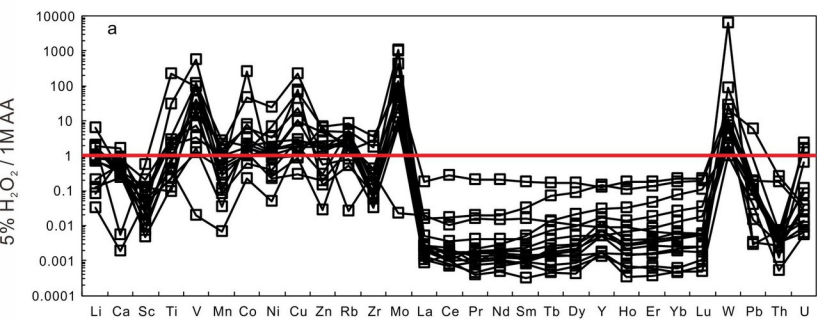
1112

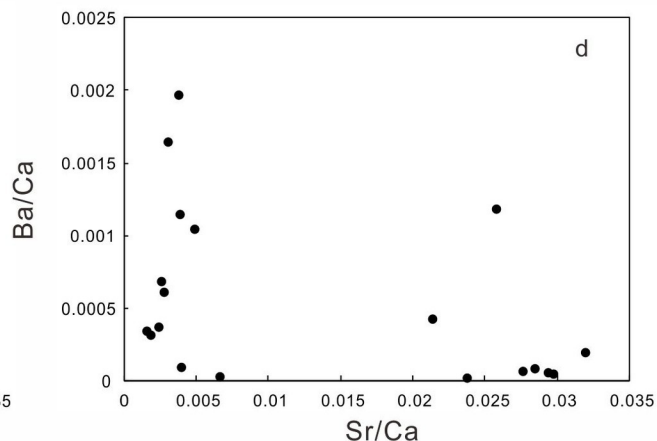
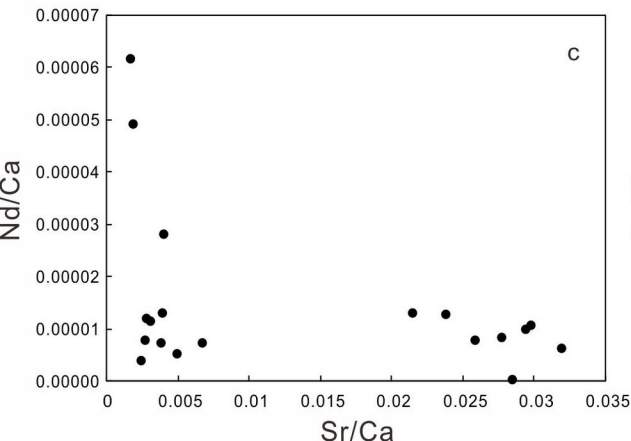
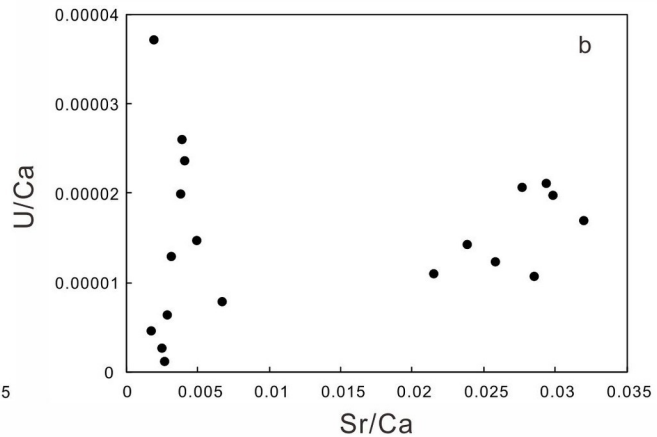
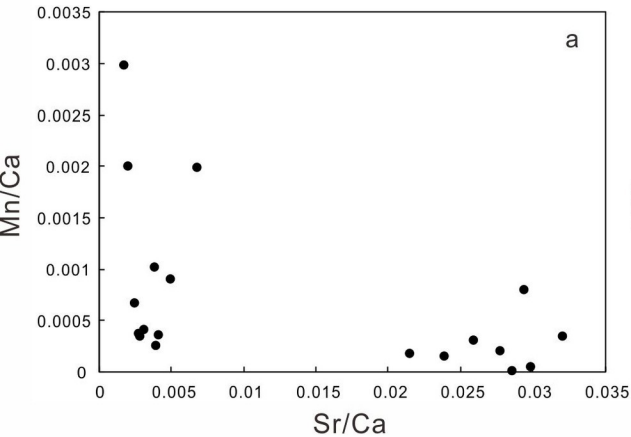
1113 **Table 4.** Concentrations of archaeal and bacterial lipids.

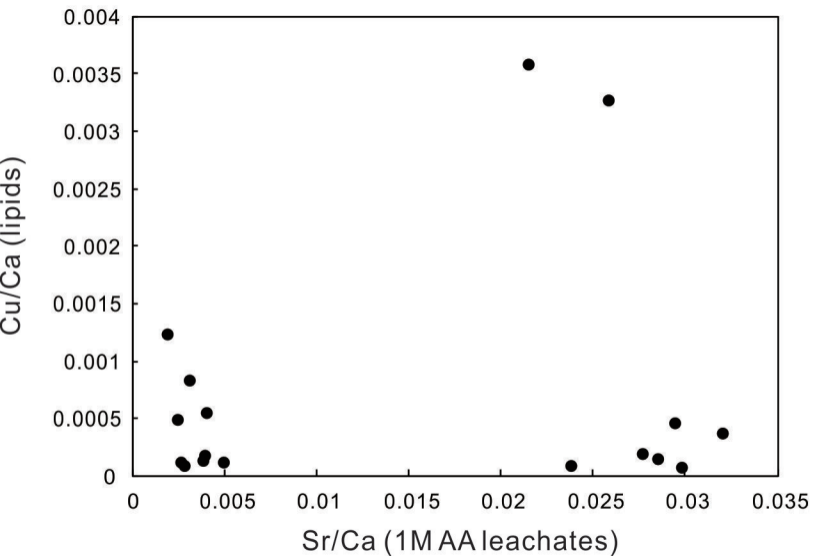
1114

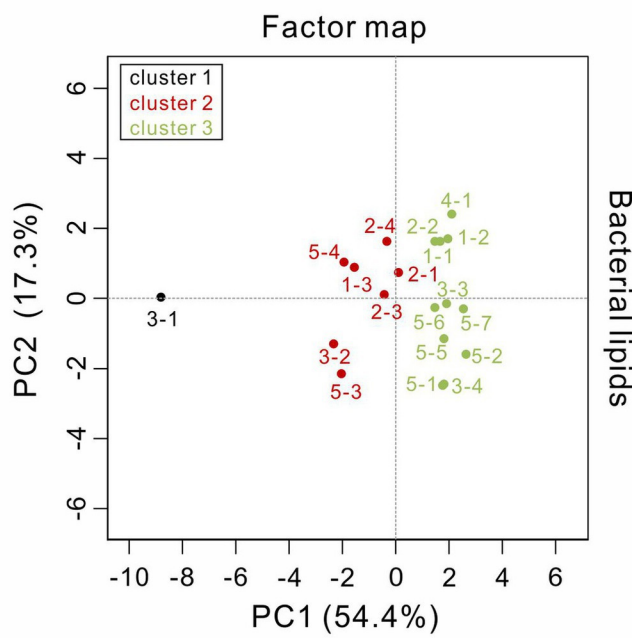
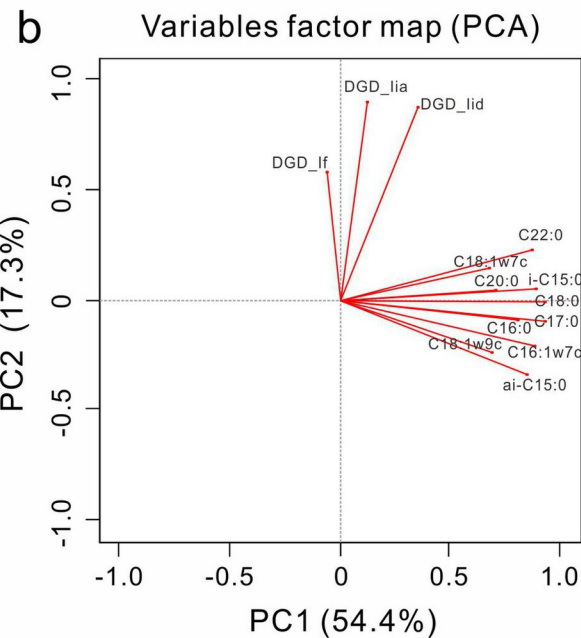
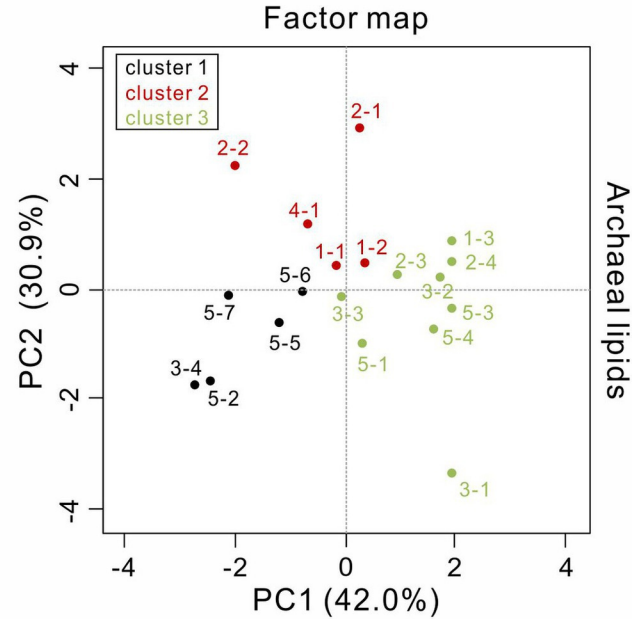
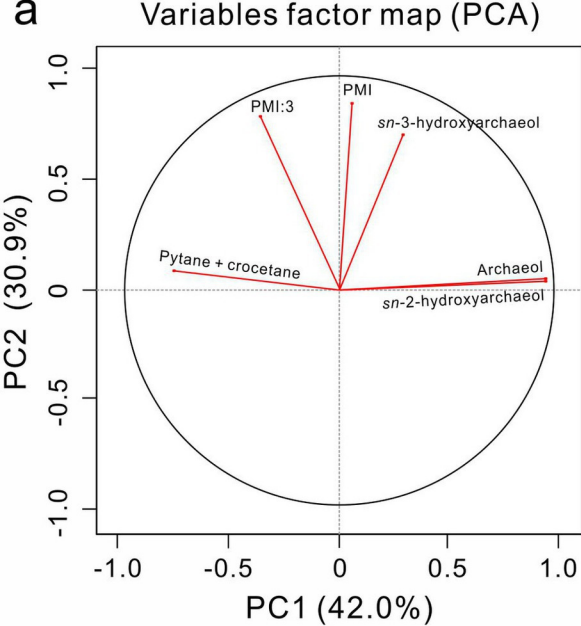












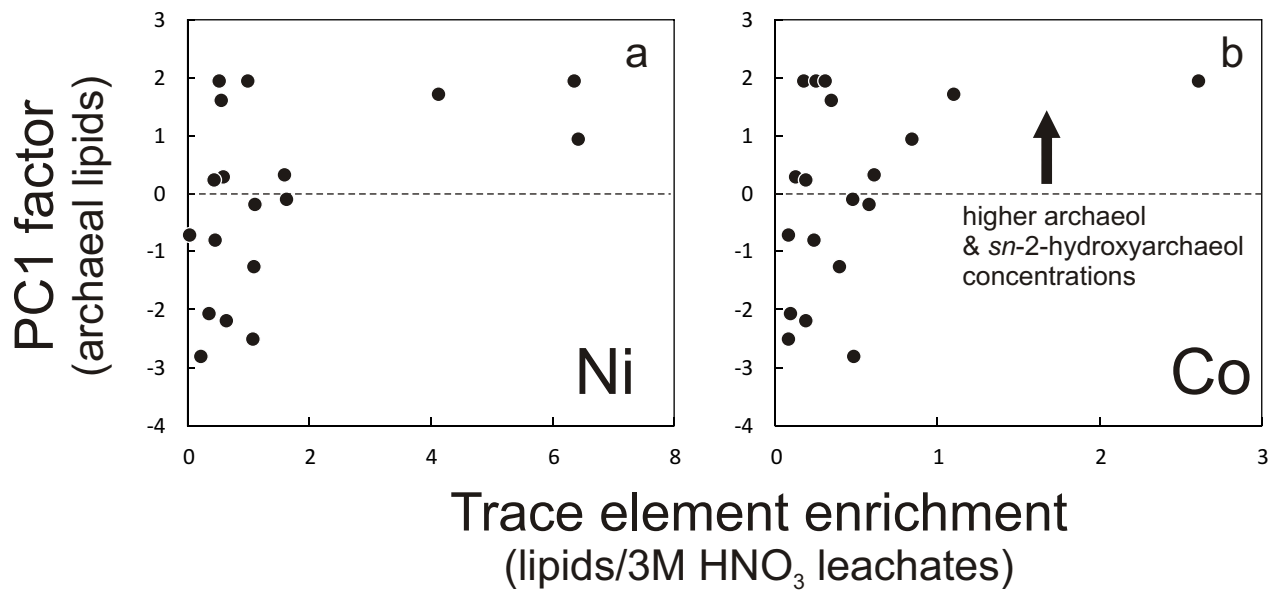


Table 1 Site information, water depth, mineral compositions, and carbon and oxygen stable isotopic compositions of the seep carbonate analyzed in this study

Sites	Area	Old ID	New ID	water depth (m)	C and O isotopes		Mineral composition			cited from
					$\delta^{13}\text{C}$ (‰)	$\delta^{18}\text{O}$ (‰)	Arag. (wt %)	Cal. (wt %)	Dolo. (wt %)	
1	Congo Fan	ZR2-PL13-P04	1-1	2830	-58.5	5.3		>50%		Pierre and Fouquet, 2007
		ZR2-PL14-P05	1-2	3150	-53.6	5.6		>50%		
		BZ1-GBT3-PL7-83	1-3	3150	-49.5	2.9		>50%		
2	Nile Deep-Sea Fan	NL4-CC1	2-1	2875-3032	-38.9	2.8	72.0	4.0	1.0	Gontharet et al., 2007
		NL7-CC1	2-2	1683-2132	-41.8	4.2	0.0	51.0	27.0	
		NL14-CC5	2-3	1683-2132	-29.2	3.2	70.0	20.0		
		NL20-CC1	2-4	2875-3032	-38.4	3.1	82.0	5.0		
3	Niger Fan	N1-KS-07	3-1	1633	-45.9	4.0	87.4	11.5		Rongemaille et al., 2011
		N1-KS-22	3-2	1150	-27.8	4.9	90.4	9.8		
		N1-KSF-45	3-3	1546	-47.1	6.1		5.7	87.3	
		N1-KI-47	3-4	1540	-48.0	5.7		7.7	86.3	
4	eastern Mediterranean Sea	MN13BT6-1	4-1	~2000	-31.0	3.9	86.8	4.1		Aloisi et al., 2000
5	Gulf of Mexico	#2 4173-2 (AT340)	5-1	2216	-54.2	4.0	62.5			Feng et al., 2010
		#7 4174-2 (GC600)	5-2	1250	-21.4	4.8		52.3		Roberts et al., 2010
		#65 271-1 (MC462)	5-3	973	-40.5	4.6	79.8			Feng et al., unpublished data
		#67 272-1 (GC415)	5-4	1110	-38.2	3.4		68.4	1.1	Feng and Roberts, 2011
		#68 273-1 (GC852)	5-5		-40.2	3.7		69.8	1.2	
		#69 273-2 (GC852)	5-6	1633	-40.1	3.7		62.0	1.5	Roberts et al., 2010
		#70 273-3 (GC852)	5-7		-48.1	4.5		54.3	1.7	

Table 2 element concentrations (mg/kg) for BHVO-2 and JLS-1

element	BHVO-2	JLS-1	
	Reference values ^a	This study	RSD (%)
Li	4.7	0.07	11.8
Ca	81429 ^b	403500 ^c	—
Sc	32.3	0.019	7.8
Ti	16364	2.75	61.0
V	317	3.00	2.4
Mn	1290	14.68	2.4
Co	45	0.045	4.9
Ni	121	0.30	4.6
Cu	123	0.15	7.3
Zn	101	2.09	2.6
Rb	9.08	0.10	5.5
Sr	396	274	2.3
Y	27.6	0.24	0.4
Zr	164.9	0.14	17.0
Mo	4.07 ^b	0.079	3.3
Ba	131	432	2.6
La	15.2	0.094	2.6
Ce	37.5	0.171	3.1
Pr	5.31	0.021	1.8
Nd	24.5	0.084	0.7
Sm	6.07	0.019	1.5
Tb	0.94	0.003	1.8
Dy	5.31	0.019	1.6
Ho	1.00	0.005	3.4
Er	2.54	0.014	4.4
Tm	0.34	—	—
Yb	2.00	0.012	3.2
Lu	0.27	0.002	2.2
W	0.22	0.10	3.5
Pb	1.51	0.08	9.1
Th	1.21	0.017	2.6
U	0.41	1.68	1.1

a: from Barrat et al. (2012)

b: from Jochum et al. (2016)

c: from Straaten et al. (2008)

Table 3 Element concentrations for inorganic and organic fractions of cold seep carbonates (mg/kg)

1M AA leachates																
New ID	Li	Ca	Sc	Ti	V	Mn	Co	Ni	Cu	Zn	Rb	Sr	Zr	Mo	Ba	
1-1	4.16	405,389	0.12	0.64	3.16	412.6	0.19	1.14	0.12	4.42	0.64	1,535	0.10	0.71	798	
1-2	2.86	289,087	0.18	0.60	7.48	76.4	0.19	0.75	0.04	1.83	0.34	1,121	0.11	0.41	330	
1-3	3.22	437,326	0.26	0.56	1.63	70.1	0.75	3.00	0.19	2.86	0.32	10,409	0.13	0.07	10	
2-1	1.29	332,078	0.38	0.31	8.79	265.5	0.54	1.90	0.24	3.87	0.76	9,753	0.77	0.18	18	
2-2	3.31	318,397	0.72	1.27	1.77	117.4	2.42	3.82	1.92	3.94	0.57	1,281	0.41	0.06	30	
2-3	2.10	355,634	0.64	0.97	3.68	63.5	0.29	1.59	3.34	5.07	0.50	7,619	0.41	0.05	152	
2-4	1.39	374,142	0.27	0.92	3.30	114.9	0.38	0.93	1.96	2.84	0.37	9,657	0.58	0.06	444	
3-1	0.62	370,540	0.01	0.30	4.67	3.9	0.03	0.72	0.21	1.53	0.12	10,563	0.02	5.13	32	
3-2	1.12	346,842	0.11	0.36	6.25	19.8	0.22	0.63	0.13	1.50	0.30	10,327	0.08	0.71	17	
3-3	3.01	209,436	2.18	0.53	14.46	419.4	0.33	1.05	0.03	6.12	1.11	395	0.47	0.19	65	
3-4	4.90	294,943	1.32	0.13	0.69	880.2	1.14	6.28	0.80	11.76	1.71	485	0.14	0.07	100	
4-1	1.50	364,923	0.30	0.18	0.63	727.6	0.81	4.98	2.71	3.07	0.28	2,442	0.10	0.06	10	
5-1	0.84	483,551	0.21	0.21	1.20	167.4	0.54	1.60	0.90	2.07	0.92	15,455	0.45	0.07	92	
5-2	2.12	440,932	0.13	0.14	1.64	294.9	0.52	1.25	0.46	3.68	0.71	1,074	0.44	0.12	162	
5-3	0.83	449,033	0.10	0.06	0.83	91.0	0.08	4.32	1.68	2.64	0.47	12,430	0.34	0.13	31	
5-4	3.88	623,116	0.13	0.09	1.39	564.1	0.60	4.73	1.23	5.44	0.74	3,051	0.12	0.09	652	
5-5	2.27	429,953	0.13	0.26	2.21	160.1	0.51	1.67	0.85	3.35	0.59	1,141	0.34	0.06	295	
5-6	2.77	521,271	0.13	0.09	1.95	181.9	0.53	3.19	1.19	3.52	0.71	1,445	0.20	0.06	318	
5-7	2.14	398,997	0.35	0.94	6.90	166.7	0.42	1.18	0.85	3.86	0.64	1,228	1.08	0.07	657	
New ID	La	Ce	Pr	Nd	Sm	Tb	Dy	Y	Ho	Er	Yb	Lu	W	Pb	Th	U
1-1	2.23	8.21	0.70	2.92	0.64	0.10	0.59	4.28	0.13	0.40	0.38	0.06	0.02	0.50	0.37	8.07
1-2	3.24	8.50	0.89	3.80	0.82	0.14	0.87	6.43	0.20	0.59	0.52	0.08	0.01	0.11	0.42	7.50
1-3	5.65	11.69	1.37	5.53	0.93	0.10	0.53	3.51	0.11	0.28	0.22	0.03	0.02	0.08	0.47	6.23
2-1	3.10	6.80	0.77	3.29	0.69	0.11	0.64	4.06	0.13	0.36	0.31	0.05	0.01	0.11	0.31	7.02
2-2	8.41	16.56	2.06	8.91	2.00	0.33	1.98	13.18	0.41	1.12	0.92	0.14	0.01	0.81	0.40	7.50
2-3	4.44	6.85	1.07	4.59	0.99	0.17	1.06	9.06	0.23	0.65	0.53	0.08	0.01	1.01	0.36	3.93
2-4	2.63	4.38	0.66	2.94	0.65	0.11	0.67	5.58	0.15	0.41	0.33	0.05	0.01	0.49	0.20	4.58
3-1	0.10	0.24	0.02	0.10	0.02	0.00	0.02	0.20	0.00	0.01	0.01	0.00	0.02	0.13	0.01	3.95
3-2	4.36	9.48	0.91	3.73	0.55	0.04	0.21	1.25	0.04	0.09	0.07	0.01	0.01	0.40	0.19	6.88
3-3	7.70	24.62	2.33	10.30	2.32	0.41	2.61	18.20	0.59	1.78	1.67	0.25	0.01	0.32	1.20	7.77

3-4	15.97	39.61	4.25	18.13	3.73	0.53	3.07	21.00	0.65	1.86	1.64	0.25	0.01	0.18	2.31	1.36
4-1	2.52	4.55	0.62	2.67	0.61	0.10	0.59	4.17	0.12	0.33	0.26	0.04	0.01	0.14	0.19	2.89
5-1	3.31	4.88	0.73	3.06	0.62	0.08	0.47	3.12	0.10	0.25	0.20	0.03	0.01	0.11	0.21	8.21

Table 3 (continued)

New ID	La	Ce	Pr	Nd	Sm	Tb	Dy	Y	Ho	Er	Yb	Lu	W	Pb	Th	U
5-2	1.84	3.17	0.41	1.74	0.38	0.06	0.37	3.00	0.08	0.23	0.21	0.03	0.01	0.03	0.07	1.19
5-3	3.83	2.43	0.85	3.73	0.66	0.07	0.38	2.32	0.07	0.19	0.14	0.02	0.01	0.29	0.08	9.30
5-4	2.90	3.60	0.70	3.20	0.75	0.12	0.69	5.49	0.15	0.39	0.31	0.05	0.01	0.06	0.07	9.13
5-5	3.33	4.54	0.77	3.39	0.75	0.12	0.73	5.62	0.16	0.43	0.35	0.05	0.01	0.13	0.09	0.50
5-6	5.99	5.92	1.39	6.26	1.42	0.24	1.42	11.07	0.31	0.83	0.64	0.10	0.01	0.22	0.09	3.35
5-7	4.94	9.38	1.11	4.53	0.95	0.15	0.88	6.20	0.19	0.52	0.46	0.07	0.01	0.14	0.44	5.17

3M HNO₃ leachates

New ID	Li	Ca	Sc	Ti	V	Mn	Co	Ni	Cu	Zn	Rb	Sr	Zr	Mo	Ba
1-1	1.28	78,284	0.49	9.51	1.85	94.8	0.37	1.94	2.05	3.81	1.32	276	0.48	0.36	862
1-2	1.18	76,201	0.54	11.78	4.18	37.9	0.47	1.61	2.06	3.51	1.27	276	0.56	0.44	110
1-3	1.72	84,464	0.76	19.23	9.27	19.9	0.58	2.16	1.13	5.13	1.01	1,757	0.66	0.36	4
2-1	0.70	82,870	0.80	15.11	10.92	107.5	1.87	3.38	5.07	4.98	1.53	1,967	4.01	2.16	5
2-2	1.39	57,396	1.15	33.08	11.93	99.9	3.84	4.44	4.11	3.34	1.21	229	3.72	0.21	10
2-3	0.82	77,181	0.72	20.93	5.83	19.9	0.32	1.53	2.59	2.85	0.85	1,534	1.23	0.05	42
2-4	0.79	86,172	0.60	14.75	4.31	38.6	0.39	1.54	2.40	2.57	0.78	1,958	1.63	0.27	1110
3-1	0.23	100,187	0.12	2.01	1.15	0.8	0.03	0.29	0.32	0.41	0.10	2,660	0.02	0.49	5
3-2	0.34	91,331	0.26	4.27	2.31	3.8	0.30	0.66	0.68	0.69	0.25	2,302	0.13	0.31	4
3-3	0.98	51,783	2.10	11.50	9.29	138.1	0.83	1.89	1.81	2.93	1.83	74	1.43	1.41	19
3-4	1.96	37,088	1.80	10.86	37.56	445.3	2.30	7.34	2.91	12.32	4.34	54	1.73	0.12	40
4-1	1.34	77,301	0.64	11.59	4.41	211.3	2.34	13.65	5.09	3.52	0.76	436	0.97	0.14	3
5-1	1.58	73,994	0.64	18.57	10.78	91.5	1.26	2.44	3.13	5.24	2.14	2,193	2.23	0.34	20
5-2	3.18	115,006	1.17	29.58	11.11	221.3	2.47	4.98	4.13	9.57	3.58	280	6.51	0.78	57
5-3	0.80	101,206	0.41	11.98	4.68	127.8	0.76	3.39	2.67	3.45	1.08	2,325	0.76	0.26	8
5-4	1.43	56,505	0.63	13.71	26.48	199.3	1.30	3.89	2.97	6.77	1.51	270	2.22	1.48	100
5-5	1.95	68,590	0.69	19.85	10.82	111.8	1.43	3.38	2.26	6.11	1.94	179	2.87	0.09	57
5-6	2.20	68,360	0.92	24.58	16.41	218.7	2.91	5.73	3.26	7.76	2.30	184	3.41	0.13	60
5-7	2.21	57,763	0.85	36.44	6.36	60.0	0.98	2.63	2.96	6.17	2.72	191	3.67	0.46	126

New ID	La	Ce	Pr	Nd	Sm	Tb	Dy	Y	Ho	Er	Yb	Lu	W	Pb	Th	U
1-1	1.00	3.46	0.30	1.20	0.25	0.03	0.20	1.52	0.04	0.13	0.13	0.02	0.0006	0.56	0.47	1.52
1-2	1.70	4.54	0.46	1.88	0.39	0.06	0.39	3.09	0.09	0.25	0.24	0.03	0.0014	0.58	0.54	1.99
1-3	2.25	5.21	0.54	2.06	0.35	0.04	0.21	1.48	0.04	0.11	0.09	0.01	0.0046	0.80	0.71	1.55
2-1	2.83	6.67	0.79	3.21	0.65	0.09	0.51	3.13	0.10	0.26	0.21	0.03	0.0021	0.81	0.51	1.73

Table 3 (continued)

New ID	La	Ce	Pr	Nd	Sm	Tb	Dy	Y	Ho	Er	Yb	Lu	W	Pb	Th	U
2-2	3.60	8.80	0.87	3.58	0.75	0.12	0.67	5.09	0.14	0.38	0.32	0.05	0.0098	1.91	0.44	1.90
2-3	1.57	2.55	0.38	1.56	0.32	0.05	0.30	2.90	0.06	0.17	0.15	0.02	0.0079	0.54	0.18	0.93
2-4	1.43	2.51	0.35	1.45	0.30	0.04	0.26	2.30	0.05	0.14	0.12	0.02	0.0079	0.57	0.23	1.21
3-1	0.08	0.16	0.02	0.06	0.01	0.00	0.01	0.10	0.00	0.01	0.00	0.00	0.0078	0.04	0.01	1.54
3-2	1.31	2.75	0.26	1.04	0.16	0.01	0.06	0.45	0.01	0.03	0.02	0.00	0.0039	0.15	0.07	1.74
3-3	3.65	11.76	1.10	4.73	1.04	0.18	1.17	9.18	0.26	0.79	0.76	0.11	0.0050	0.64	0.63	2.58
3-4	7.73	20.59	2.06	8.37	1.69	0.23	1.34	9.51	0.28	0.79	0.74	0.11	0.0075	1.96	1.90	0.39
4-1	1.03	2.04	0.25	1.05	0.23	0.04	0.21	1.79	0.04	0.11	0.10	0.01	0.0118	0.60	0.17	0.56
5-1	2.14	3.96	0.51	2.02	0.41	0.06	0.29	2.03	0.06	0.15	0.12	0.02	0.0150	1.39	0.65	1.48
5-2	2.27	4.69	0.59	2.39	0.52	0.07	0.38	2.89	0.08	0.20	0.18	0.03	0.0147	1.79	0.82	0.48
5-3	1.57	2.17	0.36	1.45	0.26	0.03	0.16	1.20	0.03	0.08	0.07	0.01	0.0225	0.93	0.23	1.80
5-4	1.79	3.32	0.46	1.87	0.39	0.06	0.31	2.40	0.06	0.17	0.15	0.02	0.0164	1.43	0.52	1.28
5-5	1.96	3.70	0.49	1.98	0.42	0.06	0.33	2.65	0.07	0.18	0.15	0.02	0.0122	1.47	0.51	0.12
5-6	3.06	5.35	0.74	3.06	0.66	0.10	0.56	4.61	0.12	0.31	0.26	0.04	0.0104	2.53	0.67	0.54
5-7	3.30	6.68	0.79	3.10	0.62	0.08	0.45	3.23	0.09	0.24	0.21	0.03	0.0056	1.42	0.83	1.22

Detrital fractions

New ID	Li	Ca	Sc	Ti	V	Mn	Co	Ni	Cu	Zn	Rb	Sr	Zr	Mo	Ba
1-1	93.6	4,371	11.5	3,453	65.0	70.1	6.08	24.0	12.6	45.4	70	931	98	1.67	22,659
1-2	101.3	1,335	12.0	4,052	74.4	64.2	6.50	25.8	11.5	43.8	72	35	125	1.56	257
1-3	107.5	947	11.5	4,421	80.5	68.2	5.83	44.4	15.3	59.0	64	63	135	4.31	396
2-1	52.0	4,073	15.5	7,421	109.0	103.4	7.75	33.9	8.1	52.7	46	163	261	5.69	204
2-2	57.7	4,699	16.5	6,905	123.6	227.9	15.93	52.2	37.2	59.2	61	91	213	24.75	209
2-3	57.6	3,466	16.0	5,832	119.9	129.2	7.82	34.7	15.7	47.7	62	113	217	1.86	231
2-4	41.2	6,165	10.5	4,062	65.0	106.2	6.13	27.2	11.4	44.0	59	1,091	144	3.96	13,128

3-3	109.4	1,890	12.8	5,623	109.0	77.4	6.73	30.3	5.9	45.7	78	92	183	5.19	239
3-4	68.4	679	10.0	3,291	176.8	210.7	9.58	31.9	5.6	66.7	68	52	118	3.31	144
4-1	55.2	3,123	16.0	4,227	99.4	162.1	9.25	80.2	22.3	47.6	80	69	128	2.59	218
5-1	46.5	3,722	11.9	3,588	154.7	90.8	4.45	16.0	5.7	42.0	102	143	116	1.22	511
5-2	54.9	2,074	12.9	3,065	120.7	97.9	4.37	16.8	3.5	34.7	111	80	109	1.69	497
5-3	49.9	3,256	12.5	3,711	132.9	100.1	4.80	28.6	21.7	47.6	102	125	123	3.12	478
5-4	59.5	2,648	12.5	3,911	133.8	177.6	6.83	29.8	12.1	58.2	120	93	125	12.18	441
5-5	51.4	2,503	12.4	3,360	110.5	117.2	6.03	18.5	10.3	41.3	107	90	129	1.21	547
5-6	53.2	3,065	12.6	4,096	130.6	145.2	7.87	23.2	15.3	49.1	123	97	131	1.81	500

Table 3 (continued)

New ID	Li	Ca	Sc	Ti	V	Mn	Co	Ni	Cu	Zn	Rb	Sr	Zr	Mo	Ba
5-7	34.0	5,087	8.1	3,164	71.5	132.8	4.63	15.7	6.8	30.3	76	134	168	1.68	510

New ID	La	Ce	Pr	Nd	Sm	Tb	Dy	Y	Ho	Er	Yb	Lu	W	Pb	Th	U
1-1	24.40	35.50	4.20	13.89	2.41	0.30	1.81	10.94	0.37	1.09	1.14	0.17	1.44	9.80	5.41	4.23
1-2	24.10	34.92	4.16	13.72	2.34	0.33	1.98	12.89	0.41	1.23	1.30	0.19	1.59	10.18	5.59	1.95
1-3	38.62	55.56	6.56	21.53	3.47	0.39	2.16	12.10	0.41	1.16	1.13	0.16	1.79	17.14	8.52	2.53
2-1	28.31	43.31	4.96	16.96	2.91	0.42	2.76	20.34	0.61	1.89	2.05	0.30	1.58	5.86	3.60	1.60
2-2	16.20	25.97	3.05	10.83	2.02	0.35	2.29	15.97	0.50	1.54	1.65	0.24	1.56	8.44	3.94	1.71
2-3	26.90	45.32	5.10	17.82	3.07	0.43	2.73	18.90	0.59	1.77	1.91	0.28	1.21	7.60	6.77	2.14
2-4	19.67	32.94	3.73	13.11	2.31	0.33	2.11	14.54	0.46	1.39	1.50	0.22	0.97	7.12	3.61	1.57
3-3	51.02	89.50	8.98	29.57	4.63	0.52	2.98	18.01	0.61	1.77	1.82	0.27	1.33	16.61	7.38	1.89
3-4	35.20	57.90	6.27	20.56	3.26	0.37	2.09	12.20	0.42	1.21	1.25	0.19	2.16	14.64	5.45	1.14
4-1	20.48	35.68	3.90	13.39	2.15	0.30	1.96	13.86	0.44	1.38	1.51	0.22	2.20	4.58	4.73	1.83
5-1	19.11	33.25	3.66	12.65	2.02	0.27	1.78	12.93	0.41	1.32	1.48	0.22	1.01	4.42	4.28	1.95
5-2	24.67	45.29	4.92	16.95	2.64	0.34	2.24	15.39	0.51	1.59	1.74	0.26	0.87	4.77	5.37	2.74
5-3	24.25	41.85	4.65	16.02	2.56	0.34	2.23	15.63	0.50	1.56	1.72	0.25	1.36	7.65	7.34	2.65
5-4	25.05	44.53	4.82	16.55	2.64	0.36	2.36	16.39	0.53	1.65	1.79	0.26	1.39	6.16	5.57	2.24
5-5	24.19	45.22	4.87	16.96	2.74	0.38	2.53	17.14	0.56	1.73	1.84	0.27	1.16	6.87	6.35	2.48
5-6	24.85	45.51	4.95	17.25	2.80	0.39	2.57	17.79	0.57	1.77	1.88	0.28	1.39	7.03	5.75	2.53
5-7	18.61	34.02	3.78	13.44	2.34	0.34	2.23	15.51	0.50	1.54	1.65	0.24	0.80	6.16	4.25	1.67

5% H₂O₂ leachates

New ID	Li	Ca	Sc	Ti	V	Mn	Co	Ni	Cu	Zn	Rb	Sr	Zr	Mo	Ba
1-1	0.14	784	0.01	0.25	0.06	2.75	0.04	0.06	0.21	10.8	0.02	4.9	0.03	0.02	2.32
1-2	2.28	267,484	0.01	1.38	107	171	8.89	18.3	9.48	9.67	1.62	525	0.02	19.7	52.4
1-3	5.19	148,388	0.01	0.46	68.0	103	4.67	9.64	4.46	3.65	0.86	442	0.03	28.2	72.6
2-1	2.36	108,335	0.01	0.51	156	26.2	1.13	2.23	2.39	2.11	0.61	1,935	0.02	1.19	2.59
2-2	2.86	226,833	0.01	0.74	214	323	4.65	9.37	5.69	5.99	2.85	4,980	0.06	57.1	8.20
2-3	3.43	97,444	0.00	0.69	136	17.0	0.36	0.36	1.00	0.96	0.74	359	0.03	1.33	4.98
2-4	2.45	158,338	0.01	0.21	75.5	9.33	0.23	0.37	5.73	4.90	0.99	2,612	0.04	0.68	37.2
3-2	0.09	275,657	0.02	1.02	45.3	10.4	0.28	4.40	8.77	9.13	0.42	6,319	0.21	96.9	36.1
3-3	0.61	119,234	0.01	0.06	22.8	15.1	1.03	1.31	2.08	0.87	0.57	3,240	0.04	13.6	6.02
3-4	9.13	497,185	0.03	4.00	387	793	8.97	9.66	1.47	3.56	8.87	780	0.25	79.1	66.2
4-1	3.04	1,924	0.17	41.3	62.3	83.0	1.45	4.42	2.68	20.7	2.41	13.6	0.35	4.78	8.63

Table 3 (continued)

New ID	Li	Ca	Sc	Ti	V	Mn	Co	Ni	Cu	Zn	Rb	Sr	Zr	Mo	Ba
5-3	5.12	159,575	0.01	0.01	99.6	29.3	21.65	1.08	1.39	0.07	1.93	2,148	0.03	1.16	6.5
5-4	0.49	147,453	0.01	0.19	4.8	549.9	1.03	4.63	11.71		1.61	3,179	0.05	6.10	21.9
5-5	1.66	132,791	0.01		265.1	135.4	0.49	2.51	1.94		1.63	500	0.02	7.54	69.4
5-7	1.50	161,386	0.01		8.7	69.9	0.45	1.29	1.52		1.22	315	0.06	1.83	40.1

New ID	La	Ce	Pr	Nd	Sm	Tb	Dy	Y	Ho	Er	Yb	Lu	W	Pb	Th	U
1-1	0.0449	0.0820	0.0107	0.0442	0.0099	0.0012	0.0063	0.0374	0.0012	0.0028	0.0023	0.0003	0.03	0.09	0.00	0.05
1-2	0.0091	0.0120	0.0016	0.0077	0.0019	0.0006	0.0043	0.0318	0.0013	0.0048	0.0064	0.0014	0.03	0.00	0.00	0.61
1-3	0.0131	0.0118	0.0029	0.0163	0.0046	0.0013	0.0111	0.1029	0.0034	0.0128	0.0168	0.0035	0.03	0.01	0.00	0.75
2-1	0.0083	0.0119	0.0013	0.0052	0.0010	0.0002	0.0009	0.0202	0.0002	0.0006	0.0007	0.0001	0.11	0.01	0.00	0.09
2-2	0.0154	0.0160	0.0022	0.0105	0.0023	0.0006	0.0043	0.0674	0.0011	0.0037	0.0039	0.0007	0.03	0.09	0.00	0.20
2-3	0.0068	0.0136	0.0014	0.0066	0.0012	0.0002	0.0015	0.0143	0.0003	0.0010	0.0010	0.0001	0.09	0.00	0.00	0.15
2-4	0.0066	0.0077	0.0011	0.0054	0.0012	0.0003	0.0019	0.0391	0.0004	0.0015	0.0016	0.0003	0.03	0.01	0.00	0.04
3-2	0.0683	0.1597	0.0179	0.0735	0.0176	0.0031	0.0185	0.1831	0.0042	0.0126	0.0118	0.0019	0.13	0.08	0.03	0.20
3-3	0.0209	0.0249	0.0009	0.0048	0.0007	0.0002	0.0011	0.0318	0.0002	0.0006	0.0008	0.0001	0.01	0.01	0.00	0.04
3-4	0.0809	0.1438	0.0176	0.0748	0.0152	0.0037	0.0304	0.3506	0.0092	0.0343	0.0438	0.0088	0.08	0.03	0.01	2.16
4-1	0.4650	1.2438	0.1292	0.5348	0.1106	0.0164	0.0979	0.5309	0.0211	0.0595	0.0590	0.0087	0.23	0.80	0.05	0.11
5-3	0.0033	0.0037	0.0006	0.0031	0.0006	0.0002	0.0010	0.0296	0.0003	0.0008	0.0009	0.0001	61.96	0.00	0.00	0.13
5-4	0.0076	0.0086	0.0006	0.0063	0.0007	0.0002	0.0013	0.0403	0.0003	0.0010	0.0007	0.0001	0.96	0.00	0.00	14.04
5-5	0.0045	0.0036	0.0004	0.0023	0.0007	0.0001	0.0006	0.0100	0.0001	0.0003	0.0002	0.0001	0.08	0.00	0.00	1.16

5-7 0.0053 0.0064 0.0010 0.0049 0.0007 0.0001 0.0006 0.0080 0.0001 0.0003 0.0002 0.0000 0.17 0.00 0.00 3.46

lipid biomarkers

New ID	Li	Ca	Sc	Ti	V	Mn	Co	Ni	Cu	Zn	Rb	Sr	Zr	Mo	Ba
1-1	27.9	19,749	0.12	13.04	1.41	24.6	0.22	2.18	2.74	13.5	1.40	77.2	0.46	0.42	634
1-2	21.7	13,741	0.10	16.99	2.61	8.3	0.29	2.60	2.38	10.1	1.01	51.9	1.04	0.52	38.0
1-3	10.1	10,002	0.10	17.58	1.96	5.9	0.15	1.17	0.94	6.5	0.68	183	0.27	0.14	8.7
2-1	17.1	9,828	0.12	26.06	1.91	15.4	0.36	1.56	4.48	10.2	0.71	208	0.92	0.67	5.4
2-2	12.9	5,209	0.07	10.14	1.10	10.0	0.38	1.65	2.86	11.2	0.57	19.8	0.34	0.20	8.2
2-3	24.4	10,589	0.07	11.98	1.27	4.8	0.27	9.84	37.9	6.8	0.68	153	0.24	0.55	8.9
2-4	16.4	6,279	0.02	3.01	0.41	3.0	0.07	1.54	20.5	12.7	0.48	87.6	0.14	0.17	163
3-1	9.79	22,032	0.02	2.58	1.66	2.1	0.09	1.87	3.21	9.3	0.84	507	0.14	2.98	13.5
3-2	32.6	51,045	0.06	8.23	2.08	7.0	0.33	2.73	3.41	23.1	1.01	1,106	0.26	0.76	28.8
3-3	31.3	2,270	0.05	1.14	0.72	5.9	0.40	3.10	2.80	7.7	0.80	3.84	0.12	0.16	2.8

Table 3 (continued)

New ID	Li	Ca	Sc	Ti	V	Mn	Co	Ni	Cu	Zn	Rb	Sr	Zr	Mo	Ba
5-1	6.76	10,240	0.07	4.78	2.13	11.8	0.17	1.48	3.79	6.3	0.82	221	0.26	0.12	8.7
5-2	9.03	7,114	0.06	4.61	9.30	10.5	0.22	5.39	3.49	46.5	0.83	28	0.34	0.14	7.9
5-3	6.94	18,461	0.08	8.38	1.79	25.6	0.24	1.81	3.59	4.0	0.89	410	0.32	0.20	12.7
5-4	8.19	22,396	0.23	24.43	8.62	58.6	0.46	2.20	2.55	8.1	2.20	104	0.99	0.63	34.4
5-5	6.60	27,418	0.29	29.35	6.39	33.5	0.57	3.75	3.35	6.3	2.62	82	1.33	0.21	33.7
5-6	6.94	23,642	0.29	27.91	6.12	49.6	0.72	2.65	2.10	4.8	2.43	72	1.40	0.19	29.9
5-7	8.25	8,983	0.09	29.55	5.25	8.5	0.19	1.73	7.49	22.2	1.00	33	0.44	0.13	19.5

New ID	La	Ce	Pr	Nd	Sm	Tb	Dy	Y	Ho	Er	Yb	Lu	W	Pb	Th	U
1-1	0.38	1.00	0.10	0.36	0.07	0.01	0.05	0.35	0.01	0.03	0.03	0.00	0.04	0.47	0.13	0.47
1-2	0.38	0.97	0.09	0.34	0.07	0.01	0.06	0.43	0.01	0.04	0.04	0.01	0.04	0.66	0.14	0.44
1-3	0.44	0.88	0.09	0.36	0.06	0.01	0.03	0.20	0.01	0.02	0.01	0.00	0.01	0.51	0.13	0.19
2-1	0.37	0.82	0.09	0.37	0.07	0.01	0.06	0.32	0.01	0.03	0.02	0.00	0.01	0.27	0.06	0.24
2-2	0.21	0.57	0.05	0.22	0.05	0.01	0.04	0.26	0.01	0.02	0.02	0.00	0.02	0.59	0.04	0.12
2-3	0.19	0.36	0.05	0.20	0.04	0.01	0.04	0.32	0.01	0.02	0.02	0.00	0.05	0.39	0.03	0.11
2-4	0.08	0.16	0.02	0.09	0.02	0.00	0.01	0.10	0.00	0.01	0.01	0.00	0.01	0.24	0.01	0.05
3-1	0.06	0.18	0.01	0.07	0.01	0.00	0.01	0.05	0.00	0.00	0.00	0.00	0.02	0.39	0.01	0.30

3-2	0.66	1.41	0.14	0.59	0.09	0.01	0.04	0.23	0.01	0.02	0.01	0.00	0.03	0.86	0.06	0.99
3-3	0.14	0.38	0.04	0.16	0.04	0.00	0.03	0.20	0.01	0.02	0.02	0.00	0.02	0.29	0.02	0.08
5-1	0.20	0.42	0.05	0.19	0.04	0.00	0.03	0.17	0.01	0.01	0.01	0.00	0.02	0.30	0.07	0.15
5-2	0.15	0.35	0.04	0.14	0.03	0.00	0.02	0.12	0.00	0.01	0.01	0.00	0.03	0.21	0.04	0.03
5-3	0.35	0.59	0.08	0.33	0.06	0.01	0.04	0.23	0.01	0.02	0.02	0.00	0.04	0.38	0.08	0.39
5-4	0.65	1.24	0.16	0.60	0.12	0.01	0.09	0.62	0.02	0.05	0.05	0.01	0.08	0.62	0.18	0.42
5-5	0.88	1.69	0.21	0.81	0.16	0.02	0.12	0.81	0.03	0.07	0.06	0.01	0.02	0.89	0.22	0.08
5-6	1.00	1.86	0.24	0.95	0.19	0.02	0.17	1.10	0.03	0.09	0.08	0.01	0.01	0.95	0.24	0.21
5-7	0.40	0.80	0.09	0.34	0.07	0.01	0.05	0.30	0.01	0.03	0.02	0.00	0.01	0.37	0.08	0.09

Table 4 Lipid biomarker results

Sites	Study locations	New ID	Archaeal lipids (mg/kg dw)					
			Pytane + Crocetane	PMI	PMI:3	Archaeol	<i>sn</i> -2-hydroxyarchaeol	<i>sn</i> -3-hydroxyarchaeol
1	Congo Fan	1-1	-	-	-	0.01	0.03	-
		1-2	-	-	-	0.03	0.04	-
		1-3	0.03	0.25	-	0.83	0.60	0.22
2	Nile Deep-Sea Fan	2-1	0.21	0.42	0.49	0.92	1.28	0.10
		2-2	0.08	-	-	-	-	-
		2-3	0.05	0.02	-	0.21	0.48	0.03
		2-4	0.02	0.03	-	0.36	0.46	0.21
		3-1	0.25	0.25	0.01	6.97	22.13	-
3	Niger Fan	3-2	0.07	0.05	-	0.73	1.34	0.20
		3-3	0.09	-	-	0.09	0.23	0.02
		3-4	0.13	-	-	-	-	-
4	eastern Mediterranean Sea	4-1	-	-	-	-	-	-
		5-1	0.17	0.09	-	0.31	0.68	0.04
		5-2	0.25	-	-	0.02	-	-
5	Gulf of Mexico	5-3	0.13	0.11	-	1.76	3.20	0.29
		5-4	0.15	0.14	-	1.48	3.08	0.09
		5-5	0.07	0.03	-	0.04	0.03	-
		5-6	0.06	0.04	-	0.06	0.04	-
		5-7	0.06	0.03	-	-	-	-

Table 4 (continued)

Sites	New ID	Bacterial lipids (mg/kg dw)												
		DGD_If	DGD_Ila	DGD_IId	<i>i</i> -C15:0	<i>ai</i> -C15:0	C16:1 ω 7	C16:0	C17:0	C18:1 ω 9	C18:1 ω 7	C18:0	C20:0	C22:0
1	1-1	-	-	-	-	-	-	0.16	-	-	-	0.21	-	0.04
	1-2	-	-	-	-	-	-	0.14	-	-	0.02	0.20	0.02	0.02
	1-3	0.43	0.07	0.11	0.01	-	0.01	0.64	0.05	0.01	0.01	0.88	0.02	0.03
2	2-1	0.17	0.16	0.22	0.05	0.02	0.05	0.23	0.03	0.07	0.14	0.39	0.04	0.02
	2-2	-	-	-	-	-	-	0.06	-	0.01	-	0.15	0.01	0.02
	2-3	-	-	-	-	-	0.01	0.22	-	-	0.02	0.18	0.01	0.02
	2-4	0.06	0.12	0.22	-	0.01	-	0.24	0.02	0.03	0.02	0.19	0.01	0.02
3	3-1	0.41	1.07	0.55	0.02	0.02	-	0.14	-	0.04	0.02	0.08	-	0.01
	3-2	0.04	-	-	-	0.01	-	0.35	-	0.01	0.01	0.30	0.01	0.02
	3-3	-	-	-	-	0.02	0.06	0.22	0.02	0.02	0.08	0.19	-	0.06
	3-4	-	-	-	-	0.05	0.12	0.87	0.05	0.16	-	0.78	0.02	0.02
4	4-1	-	-	-	-	-	-	0.09	-	-	-	0.11	-	0.01
5	5-1	0.12	-	-	0.05	0.06	0.09	1.99	0.14	0.09	0.14	1.61	0.05	0.07
	5-2	0.04	-	-	0.03	0.03	0.06	0.89	0.12	0.10	-	0.63	0.03	0.06
	5-3	0.21	-	-	0.05	0.03	-	0.62	0.05	0.02	0.05	0.46	0.02	0.01
	5-4	0.29	0.25	0.39	0.01	0.02	-	0.78	0.05	0.03	0.06	0.63	0.03	0.02
	5-5	-	-	-	0.02	0.02	-	0.76	0.02	0.03	0.05	0.61	0.02	0.02
	5-6	-	-	-	-	0.02	-	0.55	0.03	-	0.08	0.39	0.01	0.06
	5-7	-	-	-	-	0.02	-	0.45	0.05	0.02	0.04	0.36	0.02	0.07

"-" indicate not determined